Virus glycoprotein nanodisc platform for vaccine design

Kimmo Rantalainen[1,2,3], Alessia Liguori[1,2,3], Gabriel Ozorowski[3,4], Claudia Flynn[1,2,3], Jon M. Steichen[1,2,3], Olivia Swanson[1,2,3,4], Patrick J. Madden[3,5], Sabyasachi Baboo[4], Swastik Phulera[4], Anant Gharpure[4], Danny Lu[1,2,3], Oleksandr Kalyuzhniy[1,2,3], Patrick Skog[1,2,3], Sierra Terada[1,2,3], Monolina Shil[3,5], Jolene K. Diedrich[4], Erik Georgeson[1,2,3], Ryan Tingle[1,2,3], Saman Eskandarzadeh[1,2,3], Wen-Hsin Lee[4], Nushin Alavi[1,2,3], Diana Goodwin[1,2,3], Michael Kubitz[1,2,3], Sonya Amirzehni[1,2,3], Sunny Himansu[6], Devin Sok[1,2,3], Jeong Hyun Lee[1,2,3], John R. Yates III[4], James C. Paulson[1,3,6], Shane Crotty[3,5,7], Torben Schiffner[1,2,3,8,*], Andrew B. Ward[3,4,*], William R. Schief[1,2,3,6,*]

Affiliations

[1] Department of Immunology and Microbiology, The Scripps Research Institute, La Jolla, CA, USA.

[2] IAVI Neutralizing Antibody Center, The Scripps Research Institute, La Jolla, CA, USA.

[3] Consortium for HIV/AIDS Vaccine Development (CHAVD), The Scripps Research Institute, La Jolla, CA, USA.

[4] Department of Integrative Structural and Computational Biology, The Scripps Research Institute, La Jolla, CA 92037, USA.

[5] Center for Vaccine Innovation, La Jolla Institute for Immunology, La Jolla, CA 92037, USA.

[6] Moderna Inc., Cambridge, MA, 02139, USA.

[7] Division of Infectious Diseases, Department of Medicine, University of California San Diego, La Jolla, CA 92037, USA.

[8] Institute for Drug Discovery, Leipzig University Medical Faculty, Leipzig, 04103, Germany

*Corresponding authors. Email: torbens@scripps.edu (T.S.), andrew@scripps.edu (A.B.W.), or schief@scripps.edu (W.R.S.)

Abstract

Transmembrane glycoproteins of enveloped viruses are the targets of neutralizing antibodies and essential vaccine antigens. mRNA-LNP technology allows in situ production of transmembrane glycoproteins upon immunization, but biophysical characterization of transmembrane antigens and in vitro analysis of post-immunization antibody responses typically rely on soluble proteins. Here, we present a methodological platform for assembling transmembrane glycoprotein vaccine candidates into lipid nanodiscs. We demonstrate the utility of the nanodiscs in HIV membrane proximal external region (MPER)-targeting vaccine development by binding assays using surface plasmon resonance (SPR), ex vivo B cell sorting with fluorescence-activated cell sorting (FACS), and by determining the structure of a prototypical HIV MPER-targeting immunogen nanodisc in complex with three broadly neutralizing antibodies (bnAbs), including the MPER bnAb 10E8, to 3.5 Å by cryogenic electron microscopy (cryo-EM), providing a template for structure-based immunogen design for MPER. Overall, the platform offers a tool for accelerating the development of next-generation viral vaccines.

Summary

In the past two decades, nanodiscs have emerged as means to encapsulate transmembrane proteins into a stable and more native-like environment. In most cases, proteins are extracted from the membrane by detergent solubilization and then assembled into a nanodisc by removal of the detergent in presence of lipid molecules and a scaffold protein. Since the first apolipoprotein-derived membrane scaffold proteins (MSPs) were introduced, several variations and alternative scaffolds have been described, allowing for a variety of disc sizes and versatile experimental approaches[1-5]. Structural studies of membrane proteins have perhaps benefitted the most from nanodiscs, resulting in important advances in understanding of membrane protein structure-function relationship[6, 7]. They have also been used successfully in a variety of functional and biophysical approaches such as surface plasmon resonance (SPR)[8-10].

Viral glycoproteins of enveloped viruses are membrane proteins and essential targets for vaccine development. Structure-based vaccine design was an integral part of the successful

57 COVID-19 vaccine development[11-13], and a significant portion of the groundwork stemmed from
58 decades of HIV vaccine development[14]. Structure-based methods, combined with rapidly
59 advancing computational protein design approaches and mRNA lipid nanoparticle (mRNA-LNP)
60 technology, are now revolutionizing iterative vaccine development[15, 16]. Immunogen delivery by
61 mRNA-LNP expands the available immunogens to more native-like constructs that may contain
62 the membrane-proximal epitopes such as the recently developed cleavage independent NFL
63 trimers expressing HIV Env[17] and the MD39.3 gp151 Env trimer used in the HVTN302 clinical
64 trial (NCT05217641), but recombinant transmembrane glycoprotein production for biophysical
65 characterization of the immunogens remains challenging. In most studies, membrane proteins are
66 truncated before the transmembrane domain to obtain soluble ectodomains with higher expression
67 levels and easier handling and applicability in downstream analytical methods. The regions
68 excluded typically include the membrane-proximal external region (MPER), transmembrane
69 domain (TM), and intracellular C-terminal domain (CT). In influenza HA, the anchor region
70 analogous to HIV MPER joins the ectodomain as flexible linkers to three transmembrane helices
71 and allows the trimer to tilt in relation to bilayer surface[18]. Both Env MPER and HA anchor have
72 highly conserved epitopes for neutralizing antibodies (nAbs) making them attractive targets for
73 vaccine development[19-23]. Significant progress in MPER targeted HIV vaccine development has
74 been made recently with peptide-liposome formulations showing induction of heterologous
75 neutralizing antibody B cell lineages in humans, and with mRNA delivered germline-targeting
76 (GT) epitope scaffold efficiently inducing antibody precursors in non-human primates (NHPs) and
77 mice[24, 25]. Analysis of antibodies elicited by these vaccines as well as further immunogen
78 development would benefit from inclusion of the full epitope in recombinantly expressed proteins.
79 For example, recombinant proteins matching the transmembrane immunogens delivered as mRNA
80 are required for accurate immunogen assessment in iterative vaccine design methods, such as SPR
81 and structural studies. Importantly, transmembrane versions of Env may also be required for more
82 accurate representations of the glycan shield, as many neutralizing antibodies bind specifically to
83 glycans, and glycoproteins expressed as transmembrane proteins have been shown to have glycan
84 shield compositions closer to the native glycan shield[26-28].

85 Some uses of nanodiscs to support vaccine development have been demonstrated,
86 particularly in efforts to characterize the structures of HIV MPER-targeting HIV antibody epitopes
87 and transmembrane domains of virus glycoproteins in their native membrane bilayer
88 environment[29-33]. The nanodisc assembly platform presented here provides the reproducibility,
89 scalability, and accurate replication of the vaccine candidate properties that enable routine use of
90 transmembrane viral glycoproteins in key methods employed in iterative, rational vaccine design.
91 We demonstrate use of nanodiscs to measure antibody affinities by SPR, as FACS probes to sort
92 antigen-specific B cells from mouse and non-human primate (NHP) immunization experiments,
93 and for solving the cryo-EM structure of a prototype HIV boost vaccine candidate in complex with
94 three broadly neutralizing antibodies (bnAbs) that target distinct sites of vulnerability on the HIV
95 Env surface. We highlight the benefits of the approach by reporting the structure of the entire
96 protein epitope of an HIV MPER-targeting bnAb 10E8. Finally, we show the adaptability of the
97 platform to other glycoproteins by assembling engineered Ebola virus glycoprotein in nanodiscs
98 using identical conditions to HIV Env.
99

100 **Results**

101 **Glycoprotein Nanodisc Assembly and Analysis Workflow**

102 We set to establish a workflow that provides material suitable for methods commonly used in
103 rational, iterative vaccine design (Fig. 1). The workflow was set up using the engineered and highly
104 expressing HIV Env clone BG505 MD39.3 gp151[34,35] that is currently being tested in a phase 1
105 clinical trial HVTN 302 (NCT05217641). A linker, followed by an HRV3C protease cleavage site
106 and a strep tag was added to the intracellular C-terminus, leading to a nanodisc assembly construct
107 base that will hereon be referred to as Env gp151 ND (Fig. 2a-b). This construct was then used to
108 optimize the throughput and reproducibility of nanodisc production, leading to a standardized
109 workflow (Fig. 2c). In short, transmembrane glycoproteins (GPs) were expressed on the surface
110 of human FreeStyle 293-F cells, followed by detergent solubilization with TX-100-containing
111 buffer. As the transmembrane domain of viral glycoproteins is composed of only three helices –
112 one per protomer – detergent solubilization by TX-100 was not expected to disturb the quaternary

113 structure of the engineered GP trimer as indicated by the binding of structure specific antibodies
114 to extracted GPs[27, 28]. The detergent-solubilized glycoprotein was then assembled into nanodiscs
115 using the MSP1D1 scaffold with or without a biotin tag. While a variety of scaffold proteins are
116 available, we opted to reduce variables and focused on using the standard MSP1D1 scaffold for
117 all purposes. The developed "batch assembly" approach, resembling previously described "on-
118 column"[36] and "on-bead"[37] methods, facilitated reproducibility and efficient assembly while GPs
119 remained bound to the matrix. Empty nanodiscs for control experiments were produced by
120 omitting GP in the assembly step and using His-tag of the scaffold protein with NiNTA affinity
121 purification prior to SEC. Utilizing this workflow, up to 12 samples were routinely processed
122 simultaneously in five days from transfection to purified nanodisc. One liter of cells yielded
123 approximately 100 to 700 µg of pure GP nanodiscs, which was sufficient for one to three endpoint
124 assays. For example, a single production batch produced an EBOV GP nanodiscs, an HIV Env
125 nanodisc-Fab complex for cryo-EM structural studies, and eight FACS probes for B cell sorting.
126 Final GP nanodisc preparations were stable for at least three months at +4°C based on absorbance
127 at 280 nm, presence of trimeric GP in nanodisc in negative stain (ns) EM 2D class averages, and
128 activity in SPR analysis (Fig 3 b).

129 The workflow was then piloted in an immunogen development project aiming to increase
130 the affinity of MPER targeting antibody 10E8 and therefore guiding immune responses to MPER
131 domain. In the native membrane context, the C-terminal MPER helix that is targeted by the heavy
132 chain complementarity determining region 3 (CDRH3) of 10E8 is sterically occluded (Fig 2b) and
133 one of the design goals was to improve the MPER access. To this end, N-linked glycosylation sites
134 at positions N88, N618, and N625 (HxB2 numbering) adjacent to the epitope were removed at the
135 base of the trimer. An additional R696S mutation that improved 10E8 binding while maintaining
136 trimeric Env conformation was discovered by mammalian surface display library screening.
137 Earlier structural analysis indicated that R696 resides at the intersection of the three
138 transmembrane helices[29, 38]; therefore, this mutation was predicted to disrupt helix interactions and
139 further open the trimer base. The resulting construct will be referred to as Env gp151 MPER ND.
140 A negative control for MPER antibody binding and a KO FACS probe for epitope-specific B cell

141 sorting, designated as Env gp151 MPER-KO ND, was also generated (Fig. 2a). This construct
142 included MPER mutations W672A, F673R, T676R, N677I, L679M, W680E, Y681W, and
143 W683D, which were previously reported to collectively prevent the binding of MPER-targeting
144 antibodies while preserving the overall trimeric structure of Env and other bnAb epitopes[24], or
145 screened for this study to improve the expression construct. Prototypical Ebola GP immunogen
146 EBOV GP Mayinga ND was based on a construct with trimer stabilizing mutations T577P and
147 K588F[39], to which native EBOV GP TM domain and the same intracellular elements as in the HIV
148 Env constructs were added. Assembled nanodiscs generally exhibited broad peaks in SEC spectra
149 indicative of extensive glycosylation and variation in hydrodynamic radius that may result from
150 positional heterogeneity of Env in the disc, and >95% purity and bands of the expected molecular
151 weight as examined by SDS-PAGE (Supplementary Fig. 1a-b). Ns EM 2D class averages revealed
152 features typical of nanodiscs with trimeric GP with or without Fabs (Supplementary Fig. 4a). In
153 addition to the MPER targeting immunogen constructs and EBOV GP Mayinga ND, a germline-
154 targeting HIV vaccine candidate N332-GT5 gp151[40, 41] was assembled into nanodiscs using the
155 standardized workflow to test general applicability (Supplementary Fig. 2a). Mass spectrometric
156 glycan analysis using the DeGlyPHER method[42] was done prior to and after nanodisc assembly to
157 ascertain site-specific glycan occupancy and processivity of Env constructs. This analysis
158 confirmed the presence of all expected glycans as well as a high proportion of complex glycans in
159 transmembrane constructs characteristic of native, transmembrane HIV Env (Supplementary Fig.
160 1c). Germline-targeting immunogen N332-GT5 showed a higher proportion of complex type
161 glycans in soluble version of the immunogen, matching closely the glycan composition of the
162 transmembrane version. All transmembrane Envs showed higher glycan occupancy in gp41
163 subunit.
164

165 **GP nanodisc binding kinetics to antibodies measured by SPR**

166 SPR is an essential method in iterative vaccine design that measures antibody affinities to
167 engineered immunogens, assessing the effect of the designed features as well as affinities of
168 antibodies induced by vaccination (Fig 1). We set to establish scalable and reproducible conditions

169 for measuring antibody binding kinetics against transmembrane GPs in nanodiscs in three distinct
170 SPR modalities (Fig. 3a). Modality A utilized an anti-affinity tag capture strategy in which anti-
171 strep-tag antibody was covalently immobilized on the chip surface, glycoprotein nanodiscs were
172 captured using the intracellular strep tag, and Fab analytes were employed to study monovalent
173 interactions. Modality B employed a low surface density IgG capture strategy, in which anti-
174 human IgG capture antibody was first covalently immobilized, and glycoprotein-specific IgG
175 ligands were captured at reduced capture time to limit the ligand density. Glycoprotein nanodiscs
176 were then injected as analytes. In modality C, nanodisc capture is followed by IgG flow as analyte
177 instead of Fabs, allowing a high throughput scouting approach with low nanodisc sample
178 consumption but with reduced kD accuracy due to increased bivalent interaction. Establishing
179 these three modalities for nanodisc GPs allowed flexibility in experiment design based on the need
180 in iterative vaccine development step and sample availability.

181 Next, we used the GP nanodisc SPR modalities to establish baseline kinetics for
182 neutralizing and non-neutralizing monoclonal HIV Env antibodies spanning diverse epitopes (Fig.
183 3b-d, Supplementary Fig. 2b-d). Modality A measured 250 – 100 nM affinity for 10E8 to Env
184 gp151 ND design base construct (Fig. 3b) and slightly higher affinity of 36 – 42 nM using modality
185 B, indicating that the low-density capture reduced but did not eliminate the avidity effects of
186 Modality B. Using modality A, we observed 70-fold increase in 10E8 affinity (250 nM vs 3.6 nM)
187 to Env gp151 MPER ND as a result of removal of the MPER epitope-proximal glycans and the
188 mutation R696S in TM (Fig. 3c). Kinetic analysis indicated that the improved affinity in the
189 engineered immunogen was primarily attributed to a decreased off-rate (8.1×10^{-3} s^{-1} for Env
190 gp151 ND vs 3.5×10^{-4} s^{-1} for Env gp151 MPER ND. Fig. 3d). Incorporation of MPER-KO
191 mutations completely abrogated 10E8 binding. Additional MPER targeting bnAbs and bnAbs
192 targeting other epitopes on the surface of Env were also tested for more comprehensive antigenic
193 profiling. Expectedly, this confirmed binding of MPER targeting antibodies to Env gp151 ND and
194 no binding to Env gp140 (Supplementary Fig. 2b), and similar affinities of non-MPER bNabs to
195 soluble Env gp140 and Env gp151 ND (Supplementary Fig. 2c), with reduced or absent binding
196 of non-neutralizing antibodies RM19R and RM20A3 to Env gp151 ND as compared to Env gp140

197 (Supplementary Fig 2d). These two antibodies target the base of the trimer, which is exposed in
198 Env gp140, whereas in Env gp151 ND access is presumably restricted by MPER and TM domains
199 as well as the lipid surface of the nanodisc. Finally, we employed modality C to confirm the
200 binding of two Ebola GP glycan cap specific antibodies EBOV-296 and 13C6 to EBOV GP
201 nanodiscs (Fig. 3e). Collectively, these data demonstrate that GP nanodiscs and SPR can be used
202 to characterize the antigenic landscape of the designed transmembrane immunogen, inform
203 immunogen selection for in vivo studies, identify suitable complexes for structural studies by cryo-
204 EM and support GP nanodisc use as B cell sorting probes in FACS (Fig 1).
205

206 **FACS sorting of B Cells from immunized animal models using nanodisc GP probes**

207 Single B cell sorting and sequencing is routinely used to analyze B cell responses induced in vivo.
208 Typically, biotin-tagged variants of the immunogen are used with streptavidin. This allows
209 conjugation with multiple fluorochromes to increase selection specificity. By including a matching
210 sorting probe with KO mutations in the targeted epitope, epitope-specific responses can be
211 separated from off-target responses against unrelated epitopes. Soluble GP protein constructs
212 solely consisting of the ectodomain are most often used as antigenic baits. For immunization
213 studies where membrane-proximal epitopes are of interest, such as the HIV MPER, soluble probes
214 would not be able to extract all appropriate responses to the targeted epitope due to several
215 challenges which include 1) the hydrophobicity of the epitope regions which make bait production
216 challenging, 2) non-native or incomplete structural conformation of the epitope in shorter peptide
217 representations of the antigen, 3) missing lipid membrane components which constitute a portion
218 of the native epitope. Here, we used biotinylated MSP1D1 scaffold to generate nanodisc GP FACS
219 probes. We first tested Env gp151 ND probe binding to FACS compensation beads conjugated to
220 10E8, DH511 or BG18 bnAbs (Fig. 4a). Background signal was measured as binding to either
221 MSP1D1 scaffold protein alone, empty nanodisc assembled with DOPC lipids, or to empty
222 nanodisc with mixture of neutral and charged lipids. Env gp151 ND exhibited substantially higher
223 signal compared to controls, confirming that adequate separation from background signal can be
224 detected. We detected no binding with any of the tested probes to unimmunized C57BL/6 (B6)

225 mouse splenocytes, and a strong signal against engineered Ramos cells expressing the bnAb
226 VRC01 as its B cell receptor (BCR) [43]. This data indicated that Env nanodisc probes were suitable
227 for detection of B cells from mice by flow cytometry that specifically target Env.

228 We then proceeded with a pilot immunization experiment in mice to explore if vaccine
229 elicited antigen-specific B cells could be identified using Env nanodiscs probes. We utilized
230 transgenic mice expressing the human D3-3 and J_H6 genes that allow mice to express long
231 HCDR3s, including HCDR3 precursors of HIV MPER bnAbs 10E8, DH511 and LN01[24]. Mice
232 were intramuscularly injected with 10 µg of mRNA-LNPs encoding HIV Env gp151 MPER ND
233 construct. Animals were sacrificed, and spleens and lymph nodes were harvested 6 weeks post
234 immunization. B cells were stained with immunogen-matched (WT) nanodisc probes on two
235 distinct fluorophores and Env gp151 MPER-KO ND nanodisc probe with KO mutations in the
236 MPER to identify MPER-specific cells (Fig. 4b and Supplementary Fig. 3). Among class-switched
237 memory B cells (defined as $CD19^+IgD^-IgM^-$), 0.7% of cells were determined to be antigen-
238 specific, compared to 0.15% within the IgD^+IgM^+ naïve B cell population (Fig. 4c). This ~4.7-fold
239 increase was statistically significant (p=0.0177), indicating that the mRNA immunization elicited
240 HIV Env gp151 MPER -specific responses that could be detected by Env nanodisc probes. The
241 proportion of WT Env nanodisc-binding B cells that selectively bound to the 10E8 epitope (%KO^-
242 of WT^{++} B cells) was indistinguishable between the naïve and memory B cell compartments,
243 suggesting that the immunogen did not elicit MPER-specific responses, and that further
244 engineering or inclusion of a prior priming immunogen in the immunization regimen would be
245 required to achieve that capacity.

246 Antigen-specific (WT^{++}) mouse memory B cells were sorted and their BCRs sequenced to
247 assess the robustness of nanodisc probes in the selection of antigen-specific BCRs. Eight
248 antibodies from each animal were randomly selected for monoclonal antibody production. An
249 additional 12 antibodies with long (>=19 AA) CDRH3s were selected and duplicate antibodies
250 (containing identical heavy- and light chains) were removed, resulting in 54 total antibodies. Genes
251 encoding these antibodies were synthesized and 49 out of 54 antibodies were successfully
252 expressed, purified and used in SPR modality B to measure affinities against Env nanodiscs (Fig.

253 4d). At 1 μM analyte concentration, no non-specific responses to empty nanodiscs were detected.
254 Out of the tested antibodies, 47% bound to soluble gp140 matching the immunogen ectodomain
255 and 65% to Env gp151 MPER ND or Env gp151 MPER-KO ND. Considerable binding to
256 ectodomain, similar binding to MPER targeting immunogen and its MPER KO version and overall
257 similar geometric mean affinity to tested Env nanodiscs provided evidence that the elicited
258 antibodies were not targeting the MPER peptide but bound to the exposed base epitope or other
259 off-target epitopes. Nevertheless, using the nanodiscs as FACS sorting probes and in SPR, we were
260 able to sort and measure affinities of several antibodies that were specific to the transmembrane
261 Env gp151 version (e.g. Ab_38, Ab_48, Ab_79. Supplementary Fig. 3b).
262 Non-human primates (NHPs) are an important model for late-stage pre-clinical vaccine
263 development and are often used as final validation before clinical trials. Rhesus macaques, like
264 humans, have extensive genetic diversity within the immunoglobulin loci and are also capable of
265 making long CDRH3s [44-46]. To test whether nanodisc-based FACS tetramer probes could be
266 successfully used in RMs, experiments were carried out using PBMCs from animals immunized
267 previously with soluble Env MD39[47]. PBMCs were stained with the nanodisc probes to determine
268 whether there was substantial background binding to the lipid component of the nanodisc probes.
269 Pre-immunization PBMCs showed low background binding of IgD^- memory B cells to nanodisc,
270 while PBMCs from 2-weeks post an MD39 booster immunization showed high binding to the
271 nanodisc probes (Fig. 5a). Next, the nanodisc probes were compared directly to soluble Env gp140
272 protein probes in RMs that had been immunized with MD39.3 gp151 mRNA (matching Env gp151
273 ND sequence) 4-weeks prior[48]. Across two animals there were no differences in the frequency of
274 $tetramer^{++}$ cells between the Env gp151 ND nanodisc and Env gp140 soluble protein probes (Fig.
275 5b). Taken together these data show that nanodiscs bearing stabilized HIV Env constructs can be
276 deployed as tetramer probes for the evaluation of pre-clinical HIV B cell responses in NHPs.
277
278 **GP nanodiscs in cryo-EM structural studies**
279 To demonstrate how structural studies of nanodisc GPs can inform vaccine design, we set
280 out to solve the structure of prototype MPER vaccine candidate Env gp151 MPER ND in complex

281 with 10E8 antibody by cryo-EM. We included two other HIV bnAbs: VRC01, which recognize
282 the CD4 binding site, and BG18, which targets the N332 glycan supersite. This antibody cocktail
283 complex serves three purposes: First, the added Fabs improve the orientation distribution of
284 particles on cryo-EM grids. Second, they will stabilize the trimer and prevent protomers from
285 dissociating. Lastly, a functional HIV vaccine will likely require elicitation of bnAbs targeting
286 several sites to achieve sterilizing immunity. A trimer boost would therefore benefit from being
287 able to engage three or more sites (i.e. N332, CD4 and MPER) in a single immunogen. The high-
288 resolution structure of the 10E8 epitope has thus far been resolved only with x-ray crystallography
289 and in complex with MPER peptide alone[49-52]. From our cryo-EM data we produced two
290 reconstructions: the complex with two 10E8 Fabs at 4.3 Å, and the complex with a single 10E8
291 Fab at 3.5 Å resolution, which enable atomic level interpretation. We noted that while 10E8,
292 VRC01 and BG18 were all added at the same step after the nanodisc batch assembly at ~10x molar
293 excess, all VRC01 and BG18 sites were occupied but 10E8 binding site was partially
294 underoccupied in all reconstructions, suggesting steric hinderance of the MPER epitope with
295 increasing 10E8 occupancy (Fig. 6a-c). In all reconstructions, 10E8 is wedged between the Env
296 ectodomain and nanodisc lipid bilayer. MPER antibody induced Env tilt angle was evaluated by
297 aligning the low pass filtered maps to the nanodisc representing the bilayer plane. A single 10E8
298 Fab appears to be accommodated with minimal Env tilting while binding of a second 10E8 Fab
299 pushes Env into a more tilted position (Fig. 6b). Unlike in our previous WT Env AMC011 nanodisc
300 cryo-EM reconstruction, density for the TM domain remained undetected, presumably due to the
301 R696S mutation disrupting the stabilizing connection point of the three helices in the middle of
302 the bilayer[29]. The single 10E8 class was subjected to 3D variability analysis (3DVA), which
303 revealed distinct conformations of the MPER helix with ~30° lateral twist of the Fab in conjunction
304 with an apparent dislocation of the adjacent protomer (Supplementary Fig. 4c-d. Supplementary
305 video 1).

306 Using the model of Env gp151 MPER ND complex, we were able to resolve novel
307 structural details of the 10E8 epitope including a binding pocket for 10E8 antibody framework
308 region 3 (FRH3), formed by Env gp120 and gp41 subunits (Fig. 6d, inset 5). We identified 14 AA

309 in 10E8 contacting the C -terminus of gp120, helices α6 – α8 of gp41 in protomer 1, and L660 of
310 gp41 in protomer 2. These contacts are either in the binding pocket or in the helices forming a
311 collar around the termini of gp120. Strikingly, this binding pocket appeared to be targeted by the
312 CDRH3 of another HIV bnAb 3BC315, that was shown to accelerate trimer dissociation[53]. To
313 confirm this similarity in engaging the binding pocket, we solved the cryo-EM structure of Env
314 gp140 (BG505 MD39.3) in complex with BG18, VRC01 and 3BC315 Fabs to 3.1 Å resolution
315 (Fig 6f, Supplemental Fig. 4f-g). 3BC315 engages the binding pocket mainly with H100A, G100B
316 and Y100E at the tip of the CDRH3. In 10E8, the interaction is driven by I75, S74 and N76 of
317 FRH3 (Fig 6d, inset 5). The observed similarity of the binding pocket engagement led us to propose
318 that these antibodies may share a common mechanism for trimer destabilization. As part of the
319 binding pocket, both antibodies contact W623 in gp41 (Fig 6d, inset 5 and 6f), which is >99%
320 conserved across >5,000 diverse HIV strains from the LANL database (http://www.hiv.lanl.gov),
321 and has previously been shown to be part of a tryptophan clasp contributing to stabilizing four-
322 helix collar around the termini of gp120[54]. Engaging the binding pocket leads to widening of the
323 gp41 protomer-protomer gap (Fig. 6g), which would eventually lead to destabilization of the
324 contacts in the collar around the termini of gp120 and premature triggering of the fusion peptide.
325 This would normally occur during virus entry associated Env rearrangements that follow CD4
326 receptor binding. Another novel structural feature of the 10E8 antibody was the dynamic
327 remodeling of the N-terminal MPER helix, most likely driven by interactions with CDRH1 (D30,
328 N31 and W33) and CDRH2 (G52C, G53, G54, W55. Fig. 6d-e. Supplementary video 1). Root
329 mean square deviation (RMSD) of this CDRH1 and CDRH2 10E8 paratope region is 1.52 Å
330 compared to a published x-ray structure of 10E8 Fab in complex with a gp41 peptide (PDB 4G6F),
331 indicating that epitope presentation in a more native context recapitulates interactions more
332 faithfully than epitope peptide alone. In contrast, the RMSD of FRH3 between the nanodisc cryo-
333 EM complex and peptide-bound crystal structure is 0.46 Å. While the 10E8 crystal structure fit
334 well into the cryo-EM map (Supplementary Fig. 4e), we calculated an RMSD of 9.59 Å of the
335 entire MPER domain between the two structures, from the N-terminal portion of the MPER that
336 is connected to the rest of the ectodomain in the nanodisc Env cryo-EM structure. Taken together,

337 the comparison to previous crystal structures of 10E8 shows that native membrane environment
338 of Env is required for complete structural characterization of the MPER targeting antibody.
339 Observations of the native, dynamic binding mode of an MPER antibody, and structural
340 information of the entire side chain contact network will inform the development of next-
341 generation MPER targeting vaccines.
342
343 **Discussion**
344 Here we present a rigorously optimized glycoprotein nanodisc platform for vaccine design. We
345 show that the assembled GP nanodiscs enable characterization of transmembrane glycoprotein
346 vaccine candidates with key methods in rational, iterative vaccine development that have
347 traditionally been available only to soluble mimics. Applicability of the platform is demonstrated
348 by using SPR to measure antibody kinetics, FACS to characterize new vaccine designs and in vivo
349 antibody responses from preclinical experiments, and cryo-EM to provide structural guidance for
350 immunogen design.
351 In addition to confirming the assembly of EBOV GP in nanodiscs with two Ebola-specific
352 antibodies, we characterized the kinetic landscape of several HIV antibodies binding to HIV Env
353 in nanodiscs. These confirmed that glycan shield modifications and transmembrane domain point
354 mutation identified through directed evolution increased MPER-targeting bnAb 10E8 affinity to
355 prototypical HIV Env MPER-targeting immunogen Env gp151 MPER ND as compared to its
356 design predecessor. While the in vivo responses to the engineered immunogen in humanized
357 mouse model appeared to be outside the targeted C-terminal region of MPER, the identified
358 antibodies will provide guidance for further immunogen engineering. Potential targets of the
359 extracted antibodies include the engineered glycan hole or off-target epitopes at the trimer base.
360 Base of the trimer is partly occluded by the membrane, but some off-target epitopes may still be
361 accessible. This was also indicated by EM-based polyclonal epitope mapping (EMPEM) showing
362 that transmembrane gp151 Env administered as mRNA still elicits base-binding antibodies[15,48].
363 Importantly, using the biotinylated GP nanodisc as FACS probe, we were able to extract antibodies
364 targeting sites that are not fully present in the soluble form of the immunogen. While NHP

365 immunization was beyond the study's scope, we also confirmed GP nanodiscs can be used to
366 identify antigen-specific responses from NHPs, facilitating future studies. Two promising
367 approaches for overcoming the challenges in eliciting MPER targeting antibodies have been
368 recently described, namely priming with germline-targeting immunogen 10E8-GT12[24, 55] or
369 immunizing with MPER peptide alone in liposome formulation[25]. Both solutions present a more
370 accessible MPER peptide for antibody CDRH3. These immunogens can be followed by a next
371 generation Env boost immunogen designs presenting the complete epitope to guide the maturing
372 antibody toward breadth and higher neutralization potency. The analysis and nanodisc GP FACS
373 methods presented here provide vital guidance for these designs.

374 The platform enabled us to determine the structure of Env gp151 MPER ND to 3.5 Å,
375 leading to discovery of structural features that will inform the next generation of immunogens. The
376 structure confirms three HIV bnAb binding sites targeted in ongoing vaccine development projects
377 can be engaged by the same immunogen[56,24, 44]. This further demonstrated that the nanodisc
378 platform has the potential to be used in cryoEMPEM to resolve structures of membrane proximal
379 antibody epitopes from a mixture of specificities from post-immunization serum[57]. As multiple
380 epitopes are now being engineered into Env trimers for germline targeting, it is critical to
381 understand if and how they may compete or synergize. Additional value in using GP nanodiscs is
382 that, in contrast to previous structural studies using soluble mimetics of Env[40, 58], this nanodisc-
383 based structure resembles more closely the native transmembrane protein immunogen[48], which
384 may be important i.e. when assessing glycan engagement in the epitope. Glycan analysis of Env
385 Env gp151 ND and Env gp151 MPER ND agreed with earlier studies showing that when Env is
386 expressed as transmembrane protein, glycan processing resembles more closely that of the virus
387 particle with higher proportion of complex type glycans as in soluble forms[26, 27]. Unexpectedly,
388 germline targeting Env immunogen N332 GT5 deviated from the trend by displaying nearly
389 identical glycan composition in soluble and transmembrane versions of the immunogen. The most
390 significant value of the Env gp151 MPER ND complex cryo-EM structure however is in
391 characterizing the MPER epitope in unprecedented detail. We were able to resolve contacts of
392 10E8 bnAb with the Env ectodomain that have thus far remained elusive in structural studies. A

393 binding pocket for 10E8 FRH3 in the gp120-gp41 interface of the ectodomain, and CDRH1, 2 and
394 3 contacts to the entire MPER domain ending at the lipid bilayer interface, form a continuous
395 network of side chain interactions together spanning 29 AA in the paratope and 26 AA in the
396 epitope. These details can now be used as a structural template to design immunogens for improved
397 engagement of MPER antibodies. Finally, 3D variability analysis of the cryo-EM data illustrates
398 significant remodeling of the N-terminal MPER helix induced by CDRH1 and CDRH2 of 10E8.
399 While care should be taken when interpreting flexible regions, this captures detailed snapshots of
400 the native flexibility of the glycoprotein and MPER domain. The data depicts the range of
401 flexibility and may offer clues how to accommodate native glycoprotein flexibility in vaccine
402 design.
403 In conclusion, GP nanodisc platform provides a scalable and reproducible solution for a
404 more complete and native-like environment for transmembrane glycoprotein vaccine design. This
405 platform can therefore accelerate the development of next-generation transmembrane GP based
406 vaccines.
407
408 **Methods**
409 This method description aims to provide a complete platform that enables routine use of nanodisc
410 approach for iterative vaccine design using viral glycoproteins. While retaining the versatility of a
411 modular approach, each step is simplified and validated for maximizing reproducibility and
412 scalability.
413
414 **Protein expression and nanodisc assembly**
415 All glycoprotein and antibody constructs were codon optimized for expression in human cells and
416 synthesized and cloned into expression vectors pHLSec (glycoproteins) or its variants pCW-CHIg-
417 hG1, pFabCW pCW-CLig-hL2 or pCW-CLig-hk (IgG heavy chains, Fab heavy chains, lambda
418 light chains and kappa light chains, respectively) by GenScript Biotech. Antibodies were expressed
419 and purified from HEK293F or ExpiCHO cells according to manufacturer's instruction using
420 rProtein A Sepharose Fast Flow resin (Cytiva) as described earlier[24, 44].

421 Soluble Env GP were purified as described earlier[40]. Transmembrane glycoprotein
422 purification method was modified from the earlier protocol[29]. For one liter of transfected cells, 1
423 mg of DNA was mixed with 25 ml of OPTI-MEM medium and sterile filtrated through 0.22 µm
424 filter unit. 3 mg of PEI MAX (Polysciences, #24765) was separately mixed with 25 ml of OPTI-
425 MEM, filtrated and then combined with the DNA. Combined DNA and PEI MAX were then added
426 to HEK293F cells at 1 million/ml density and cells were incubated at 37 °C, 8% CO_2, and 80%
427 humidity under shaking at 180 rpm for 3 days. Cells were harvested by centrifugation at 1500 rcf
428 in 4 °C for 15 min, washed with ~300 ml cold PBS, and centrifuged again at 1500 rcf in 4 °C for
429 15 min. Pelleted cells were lysed with ~5 ml of lysis buffer per gram of cells (50 mM Tris-HCl
430 (pH 7.4), 300 mM NaCl, 0.5% TX-100). Prior to use, approximately 1 protease inhibitor cocktail
431 tablet per 50 ml of lysis buffer, and 2 ml of BioLock (IBA Lifesciences, # 2-0205-050) per liter of
432 cells was added to lysis buffer. Cells were lysed for 1 h at 4 °C in an overhead rotating mixer.
433 Lysed cells were centrifuged for 1 h at 25,000 rcf, followed by filtration of the supernatant through
434 0.22 µm bottle top filtration unit. This resulted in cleared lysate that was passed through Strep-
435 tactin XT 4Flow matrix (IBA Lifesciences, #2-5010-025) in a gravity flow column. Approx. 400
436 µL of drained matrix was used per liter of cells. Matrix was then washed three times with 2 ml of
437 wash buffer 1 (50 mM Tris-HCl (pH 7.4), 300 mM NaCl, 0.1% (w/v) CHAPS, 0.03 mg/mL
438 deoxycholate), three times with 2 ml of wash buffer 2 (50 mM Tris/HCl pH 7.4, 500 mM NaCl, 1
439 mM EDTA, 0.1% DDM, 0.01% CHS, 0.03 mg/ml deoxycholate) and three times 2 ml of wash
440 buffer 3 (50 mM Tris/HCl, pH 7.4, 150 mM NaCl, 0.02% DDM, 0.002% CHS, 0.03 mg/ml
441 deoxycholate). After this, matrix with detergent solubilized GP was transferred to a 5 ml test tube
442 for nanodisc assembly step.
443 Lipid stocks were prepared prior to disc assembly in 1 mM final concentrations. Premade
444 10% DDM/ 0.1% CHS stock (Anatrace, #D310-CH210) was used throughout the study. All lipids
445 in this study were prepared from chloroform stocks (Avanti Polar Lipids). Chloroform was first
446 evaporated under gentle nitrogen stream until transparent film was formed around the glass vial.
447 Lipid film was then rehydrated for 1 h in room temperature in lipid rehydration buffer (50 mM
448 Tris/HCl, pH 7.4, 150 mM NaCl, 0.1% DDM, 0.01% CHS) in a volume bringing the lipid stock

449 concentration to 5 mM. After thorough mixing by vortexing, this stock was diluted further to final
450 lipid stock solution at 1 mM concentration and sonicated with microtip (20-25% intensity, 50%
451 time cycles in 4 °C) until clear. Most lipid stock solutions cleared within 10 – 20 min but with
452 some lipids DDM/CHS amount was increased up to 1%/0.01%. 1 mM lipid stocks were aliquoted
453 and stored up to 6 months at -20°C. A lipid mix roughly following HIV particle lipid composition
454 was used throughout the study and contained 45% DOPC, 7% DOPS, 7% DOPA, 7% DOPE, 7%
455 DOPG, 5% sphingomyelin, 2% PI(4,5)P2, and 20% CHS. Scaffold protein was either produced
456 in-house using standard *E. coli* expression method or purchased from Sigma-Aldrich (membrane
457 scaffold protein 1D1 #M6574 or biotinylated membrane scaffold protein 1D1 BTN #MSP13).
458 Nanodisc batch assembly was done as follows. Strep-tactin matrix with GP bound was
459 drained by gravity flow, after which gravity flow column was capped and 400 µl of wash buffer 3
460 was added to the matrix. 50% matrix slurry was then transferred to a 5 ml test tube. Lipids were
461 added at approx. 350X molar excess and scaffold at 6X molar excess in relation to the glycoprotein.
462 Glycoprotein amount bound to the matrix was estimated with a separate initial experiment where
463 protein was eluted after the last wash step. Minor variations were made to glycoprotein:scaffold
464 and glycoprotein:lipid ratios without significant difference in the final yield. Matrix with
465 glycoprotein, lipids and scaffold was incubated for 1 h at 4°C prior to addition of SM-2 bio-beads
466 (Bio-Rad, #1523920). Bio-beads were activated according to the manufacturer's instructions in
467 methanol followed by extensive wash with deionized water. Bio-beads were added to approx. 50%
468 v/v with the nanodisc assembly mixture. i.e. if the total volume of the assembly reaction was 1.5
469 ml, final volume after bio-bead addition in the 5 ml test tube was ~3 ml. Detergent was then
470 removed by incubation in a rotating shaker overnight at 4°C. The following day an additional
471 ~20% of the total reaction volume of fresh bio-beads were added, followed by an additional 1 h
472 incubation at room temperature to ensure complete removal of detergent. Next, contents of the test
473 tube were transferred to a new gravity flow column with a pipette tip with the first ~2 mm cut off
474 to allow pipetting biobeads and matrix. Mixture was washed in column twice with 4 ml of TBS
475 and eluted with Strep-tactin elution buffer BXT in 500 µl fractions. A280 of eluted fractions were
476 monitored and fractions containing protein were pooled and concentrated to <500 µl for SEC

477 performed using a Superose 6 Increase 10/300 column (Cytiva) at 0.75ml/min in TBS. SDS-PAGE
478 and ns EM analysis were used to confirm presence of glycoprotein and scaffold protein, typical
479 disc appearance in ns EM 2D class averages and glycoprotein on disc.
480 For structural biology purposes, Fabs were added to the GP nanodiscs after the assembly
481 while nanodisc was still bound to strep-tactin matrix. After the second addition of bio-beads, each
482 Fab was added at ~10X molar excess and the mixture was incubated for an additional 2h at room
483 temperature. Complex elution and following steps were identical as described above for
484 unliganded glycoprotein nanodiscs. Fractions were pooled after SEC and sample was concentrated
485 either to 1 mg/ml for FACS, SPR and other purposes, or up to 11 mg/ml for cryo-EM sample
486 preparation.
487
488 **Identification of R696S mutation on HIV Env by mammalian directed evolution.**
489 A 250 amino acid long site-saturation mutagenesis (NNK) scan of gp41 was synthesized at SGI-
490 DNA. A fragment of the library containing NNKs from positions T606 to F699 (94 positions) was
491 cloned into BG505 MD39.2 gp151. This library was stably integrated into 293T-rtTA3G cell line
492 using the lentivirus-based mammalian display protocol described previously[34, 40,35]. After inducing
493 library expression overnight, the cells were stained with 10E8 IgG and PGT145 Fab and those
494 with highest binding to 10E8 that were also positive for PGT145 were sorted. After three rounds
495 of sorting, the library DNA was extracted and sequenced by Sanger sequencing. 8 of 19 sequences
496 had a mutation at position 696, which was mutated from R to S, A, V, I and L. The most frequent
497 mutation, R696S, was selected for further characterization.
498
499 **Mass spectrometry**
500 **Proteinase K treatment and deglycosylation.** HIV Env glycoprotein (when membrane bound,
501 denatured in 6 M urea) was exchanged to water using Microcon Ultracel PL-10 centrifugal filter.
502 Glycoprotein was reduced with 5 mM tris(2-carboxyethyl)phosphine hydrochloride (TCEP-HCl)
503 and alkylated with 10 mM 2-Chloroacetamide in 100 mM ammonium acetate for 20 min at room
504 temperature (RT, 24 °C). Initial protein-level deglycosylation was performed using 250 U of Endo

505 H for 5 µg trimer, for 1 h at 37 °C. Glycoprotein was digested with 1:25 Proteinase K (PK) for 30
506 min at 37 °C. PK was denatured by incubating at 90 °C for 15 min, then cooled to RT. Peptides
507 were deglycosylated again with 250 U Endo H for 1 h at 37 °C, then frozen at –80 °C and
508 lyophilized. 100 U PNGase F was lyophilized, resuspended in 20 µl 100 mM ammonium
509 bicarbonate prepared in $H_2{}^{18}O$, and added to the lyophilized peptides. Reactions were then
510 incubated for 1 h at 37 °C, subsequently analyzed by LC-MS/MS.
511
512 **LC-MS/MS.** Samples were analyzed on an Q Exactive HF-X mass spectrometer. Samples were
513 injected directly onto a 25 cm, 100 µm ID column packed with BEH 1.7 µm C18 resin. Samples
514 were separated at a flow rate of 300 nL/min on an EASY-nLC 1200 UHPLC. Buffers A and B
515 were 0.1% formic acid in 5% and 80% acetonitrile, respectively. The following gradient was used:
516 1–25% B over 160 min, an increase to 40% B over 40 min, an increase to 90% B over another 10
517 min and 30 min at 90% B for a total run time of 240 min. Column was re-equilibrated with solution
518 A prior to the injection of sample. Peptides were eluted from the tip of the column and nanosprayed
519 directly into the mass spectrometer by application of 2.8 kV at the back of the column. The mass
520 spectrometer was operated in a data dependent mode. Full MS1 scans were collected in the
521 Orbitrap at 120,000 resolution. The ten most abundant ions per scan were selected for HCD
522 MS/MS at 25 NCE. Dynamic exclusion was enabled with exclusion duration of 10 s and singly
523 charged ions were excluded.
524
525 **Data Processing.** Protein and peptide identification were done with Integrated Proteomics
526 Pipeline (IP2). Tandem mass spectra were extracted from raw files using RawConverter [59] and
527 searched with ProLuCID[60] against a database comprising UniProt reviewed (Swiss-Prot) proteome
528 for Homo sapiens (UP000005640), UniProt amino acid sequences for Endo H (P04067), PNGase
529 F (Q9XBM8), and Proteinase K (P06873), amino acid sequences for the examined proteins, and a
530 list of general protein contaminants. The search space included no cleavage-specificity.
531 Carbamidomethylation (+57.02146 C) was considered a static modification. Deamidation in
532 presence of $H_2{}^{18}O$ (+2.988261 N), GlcNAc (+203.079373 N), oxidation (+15.994915 M) and N-

533 terminal pyroglutamate formation (–17.026549 Q) were considered differential modifications.
534 Data was searched with 50 ppm precursor ion tolerance and 50 ppm fragment ion tolerance.
535 Identified proteins were filtered using DTASelect2[61] and utilizing a target-decoy database search
536 strategy to limit the false discovery rate to 1%, at the spectrum level[62]. A minimum of 1 peptide
537 per protein and no tryptic end per peptide were required and precursor delta mass cut-off was fixed
538 at 15 ppm. Statistical models for peptide mass modification (modstat) were applied. Census2[63]
539 label-free analysis was performed based on the precursor peak area, with a 15 ppm precursor mass
540 tolerance and 0.1 min retention time tolerance. "Match between runs" was used to find missing
541 peptides between runs. Data analysis using GlycoMSQuant [42] was implemented to automate the
542 analysis. GlycoMSQuant summed precursor peak areas across replicates, discarded peptides
543 without NGS, discarded misidentified peptides when N-glycan remnant-mass modifications were
544 localized to non-NGS asparagines and corrected/fixed N-glycan mislocalization where
545 appropriate.
546
547 **SPR**
548 The kinetics and binding affinities of antibody-antigen interactions were analyzed using either
549 ProteOn XPR36 system (Bio-Rad) or Carterra LSA. TBS pH 7.4 (20 mM Tris, 150 mM NaCl)
550 supplemented with BSA at 1 mg/ml without detergents was used as running buffer in all
551 experiments. In ProteOn XPR36, HC30M XanTec sensor chips were utilized. In modalities B and
552 C, anti-human IgG (Fc) antibody (GE, #BR-1008-39) was used for capturing IgG (ligand) at low
553 densities with nanodisc GP as the analyte. In modality A, anti-Strep-tag antibody (pAb, rabbit,
554 GenScript, #A00875) was used for capturing Strep-tagged nanodiscs GP (ligand) followed by GP
555 specific Fab as the analyte. Approximately 6000-8000 response units (RU) of the capture antibody
556 were covalently attached to the sensor surface using EDC-NHS chemistry. For IgG-antigen
557 interaction studies, approximately 50 to 100 RUs of IgGs at a concentration of 0.3 μg/ml were
558 immobilized on each flow cell. For Fab-antigen interaction studies, approximately 300 to 400 RUs
559 of antigen at 10 μg/ml were captured on each flow cell. Analytes were introduced to the flow cell
560 at a rate of 30 μl/min for 3 minutes, followed by a dissociation phase of 5 minutes. Regeneration

561 was performed with 1.7% or 0.85% phosphoric acid, each with a contact time of 60-180 seconds,
562 repeated four times per cycle. Data analysis was conducted using ProteOn Manager software (Bio-
563 Rad), including raw sensogram processing, interspot referencing, and column double referencing.
564 Equilibrium or kinetic fits were performed using the Langmuir model as needed.
565
566 Kinetics and affinity of antibody-antigen interactions on Carterra LSA using CMDP Sensor Chip
567 (Carterra) for capture IgG – flow nanodisc (modality B) was done as follows. Chip surfaces were
568 prepared according to Carterra software instructions. In a typical experiment approx. 500-700 RU
569 of capture antibody (SouthernBiothech, # 2047-01) in 10 mM Sodium Acetate pH 4.5 was amine
570 coupled on CMDP chip placing special care on concentration range of the amine coupling reagents.
571 We used N-Hydroxysuccinimide (NHS) and 1-Ethyl-3-(3-dimethylaminopropyl)
572 carbodiimidehydrochloride (EDC) from Amine Coupling Kit (GE, #BR-1000-50). Highest
573 coupling levels of capture antibody were achieved by using 10 times diluted NHS and EDC during
574 surface preparation runs as compared to kit instruction (10 ml of water each to give 11.5 mg/ml
575 and 75 mg/ml respectively according to kit instructions). Thus, the concentrations of NHS and
576 EDC were 1.15 mg/ml and 7.5 mg/ml and the activation time was reduced to 1 min. The
577 concentrated stocks of NHS and EDC were stored frozen in -20 °C for up to 2 months without
578 noticeable loss of activity. The capture antibody was used at concentration 25 µg/ml with 10
579 minutes contact time. Phosphoric Acid 1.7% was used as a regeneration solution with 60 seconds
580 contact time and injected three times per cycle. Concentration of ligands were approximately 1
581 µg/ml and contact time was 5 min. Raw sensograms were analyzed using Kinetics software
582 (Carterra) with interspot and blank double referencing, and Langmuir model. Analyte
583 concentrations were quantified on NanoDrop 2000c spectrophotometer using absorption signal at
584 280 nm. Analytes were buffer exchanged into the running buffer using dialysis. In a typical run,
585 we covered a broad range of affinities and used two referencing practices depending on the off-
586 rate of the ligand. For fast off-rate (faster than 9×10^{-3} 1/s), we use automated batch referencing
587 that includes overlay y-aline and higher analyte concentrations. For slow off-rates (9×10^{-3} 1/s or
588 less), we use manual process referencing that includes serial y-align and lower analyte

589 concentrations. After automated data analysis by Kinetics software, we performed additional
590 filtering to remove datasets with highest response signals smaller than signals from negative
591 controls using R-script.
592
593 **FACS**
594 **Validation of Env-Nanodisc proteins as fluorescent baits**
595 Streptavidin (SA) conjugated-antigen baits were prepared by combining biotinylated Env-
596 nanodisc or empty nanodisc with fluorescent SA at room temperature for at least 1 hr in dark at a
597 bait:SA molar ratio of 2:1. Control breads for FACS were generated by conjugating various bnAbs
598 to compensation beads. Mouse anti-human IgG (BD Biosciences, # 555784) was first captured on
599 to anti-mouse IgK compensation beads (BD Biosciences, # 552843), followed by a wash step and
600 a secondary capture of bnAbs of interest. VRC01-expressing Ramos cells [43], C57BL/6 splenocytes,
601 and the prepared bnAb-conjugated beads were incubated with the nanodisc GP:SA baits at a bait
602 concentration of 10-50 nM in the final staining volume for 30 min at 4 °C in the dark. Data were
603 acquired on a BD FACS Melody, and analzyed in FlowJo v10 (FlowJo, LLC).
604
605 **Mouse immunization studies**
606 hD3-3/JH6 mice were immunized as previously described[24]. Briefly, homozygous hD3-3/JH6
607 mice were injected with 10 µg (50 µl total volume) of Moderna mRNA LNPs encoding Env gp151
608 MPER I.M. under anesthesia (5% isoflurane induction) in the left quadriceps muscle. After six
609 weeks, mice were euthanized with compressed CO_2 (100%) in a clear chamber to allow for
610 visualization of respiration and subsequent death via respiratory cessation. Blood was collected
611 from the chest cavity prior to the removal of the spleen and lymph nodes (mesenteric, inguinal,
612 and popliteal). Tissues were placed in 3 mL FACS buffer (1 X PBS Ca/Mg^{++} free, 1 mM EDTA,
613 25 mM HEPES, pH 7.0, 1% heat-inactivated FBS) on ice and tissues were disassociated using the
614 rough ends of two sandblasted microscope slides, followed by centrifugation (460 rcf for 5 minutes
615 at 4 °C). Red blood cell lysis was performed using 1 mL of ACK buffer (Quality Biological) for 2
616 minutes on ice before lysis was halted by adding 14 mL FACS buffer per sample. Post lysis and

617 centrifugation (460 xg for 5 minutes), cells were resuspended in 3 mL Bambanker freezing
618 medium (Bulldog Bio) prior to filtration through a cotton-plugged, borosilicate pasteur pipette into
619 a borosilicate glass test tube. 1 mL filtered-cell solution was subsequently divided into three
620 cryovials/mouse, which were precooled in a styrofoam rack on dry ice. Cells were stored at -80 °C
621 for 2-7 days prior to long-term storage in liquid nitrogen. All work followed IACUC guidelines
622 associated with animal protocol number 20-0001.
623
624 **Mouse sample preparation and B cell sorting**
625 Mouse frozen mouse splenoctyes and lymphocytes were thawed and stained as previously
626 described[24, 56]. Briefly, after thawing and counting, total B cells were isolated by negative selection
627 using the EasySep Mouse Pan-B Cell Isolation Kit (StemCell, #19844) according to
628 manufacturer's instructions. SA-conjugated baits were prepared as described above. Wildtype
629 antigen baits were conjugated to BV421-SA (BioLegend, #405225) and AlexaFluor 647SA
630 (Invitrogen, #S21374), while epitope knockout (KO) baits were conjugated to hashtagged
631 TotalSeq-C PE SA (BioLegend, #405261). Purified B cells were stained at 4 °C in dark, with
632 appropriate baits and antibody master-mix consisting of FITC anti-CD19 (BioLegend, #152404),
633 BV786 anti-IgM (BD Biosciences, #743328), PerCP-Cy5.5 anti-IgD (BD Biosciences, #564273),
634 APC-Cy7 anti-F4/80 (BioLegend, #123118), APC-Cy7 anti-CD11c (BD Biosciences, #561241),
635 APC-Cy7 anti-Ly6C (BD Biosciences, #557661), APC-H7 anti-CD8a (BD Biosciences,
636 #560182), and APC-H7 anti-CD4 (BD Biosciences, #560181), all used at 1:100 dilution and
637 prepared in FACS buffer (1% v/v heat inactivated FBS, 1 mM EDTA, 1 mM HEPES in 1x DPBS).
638 The KO bait was first added to cells with the antibody master mix for 15 minutes, followed by the
639 addition of WT baits for an additional 30 min. Each bait was used at final bait concentration of
640 100 nM in the staining volume or 0.5 µg per sample. During the addition of antibody master mix,
641 a unique TotalSeq-C anti-mouse hashtag antibody (BioLegend) was added to each sample at a
642 concentration of 2.5 µL / up to 20 million cells. Following antibody staining, 1 mL of 1:300
643 live/dead stain diluted in FACS buffer (Invitrogen, #L34966) was added to each sample for an
644 additional 15 minutes at 4 °C, then washed with 10 mL of FACS buffer. Cells were resuspended

645 in a final volume of 500 µL FACS buffer and sorted on a BD FACS Melody. Cells were bulk
646 sorted into a 4 °C chilled PCR plate well containing 20 µL of 0.2 µm filtered FBS, and processed
647 for BCR sequencing via the 10x Genomics Single Cell Immune Profiling according to kit
648 protocols, with minor modifications outlined previously[64]. Pooled libraries were sequenced on an
649 Illumina NextSeq 2000 using a 100-cycle P3 reagent kit (Illumina, #20040559).
650

651 **BCR sequence analysis**

652 Sequence analysis Raw sequencing data were demultiplexed, processed into assembled VDJ
653 contigs and counts matrix files, and assigned to specific animal IDs based on TotalSeq-C antibody
654 hashtag counts using Cell Ranger (v6.1) and scab as previously described[64]. Gene assignment,
655 annotation, and formatting into Adaptive Immune Receptor Repertoire (AIRR) format[65] for paired
656 heavy and light chain antibody sequences was performed using Sequencing Analysis and Data
657 library for Immunoinformatics Exploration (SADIE) with a previously described custom germline
658 reference database that included all known mouse antibody genes plus the human IGHD3-3 and
659 IGHJ6 genes that were knocked into hD3-3/JH6 mice[24]. Eight antibodies from each animal were
660 randomly selected for in vitro analysis, except for one animal from which only two total
661 heavy/light pairs were recovered. In addition, 12 antibodies with long HCDR3s (>19 aa) were
662 selected for in vitro characterization.
663

664 **NHP Flow Cytometry**

665 Frozen NHP PBMC samples were thawed in RPMI media with 10% FBS, 1% GlutaMAX,
666 and 1% Penicillin/Streptomycin (R10). NHP samples used in this study were from animals that
667 were reported in previous studies [47,48]. The recovered cells were then stained with the appropriate
668 antibody panel. Fluorescent antigen probes were constructed by combining fluorophore-
669 conjugated streptavidin and biotinylated nanodisc GP or soluble Env probes with an appropriate
670 volume of PBS in small increments across 45 minutes at room temperature (RT). Thawed cells
671 were incubated with probes for thirty minutes at 4°C. A master mix of surface staining antibodies
672 was then added and incubated for thirty minutes at 4°C. Cells were washed and prepared for

673 acquisition on Cytek Aurora (Cytek Biosciences). The following reagents were used in the
674 PBMC staining panel: Alexa Fluor 647 Streptavidin (BioLegend #405237), BV421 Streptavidin
675 (BioLegend #405225), PE Streptavidin (BioLegend #405245), PE-Cy7 Streptavidin (BioLegend
676 #405206), BV711 Streptavidin (BioLegend #405241), BUV615 Streptavidin (BioLegend
677 #613013), Viability eFluor780 (1:2000, Invitrogen #65-0865-14), CD3 BV510 (1:100, BD
678 Biosciences #569488), CD14 BV510 (1:100, BioLegend #301842), CD8a BV510 (1:100, BD
679 Biosciences #563256), CD16 BV510 (1:100, BioLegend #302048), CD20 (1:100, BUV395 BD
680 Biosciences #563782), IgG BV605 (1:100, BD Biosciences #563246), and IgD AF488 (1:50,
681 Southern Biotech #2030-30).
682
683 **EM**
684 Negative stain EM was used for quality control of nanodisc assembly and for initial assessment of
685 antibody complexes for cryo-EM. Glycoprotein nanodisc or nanodisc with three fold molar excess
686 of Fab was applied to 400 mesh size Cu grid at 0.04-0.06 mg/ml concentration, blotted off with
687 filter paper and stained with 2% uranyl formate for 60 s. NsEM data was collected on a Tecnai
688 Spirit microscope operating at 120 keV, using a Tietz 4k × 4k TemCam-F416 CMOS camera and
689 Leginon automated image collection software[66]. Data was processed using Relion 3.0 image
690 processing pipeline[67].
691 For cryo-EM, nanodisc was complexed with 10X molar excess of VRC01, BG18 and 10E8 Fabs
692 after batch nanodisc assembly, while bound to affinity matrix. Eluted complex was then SEC
693 purified (Superose 6 Increase column. Cytiva), concentrated to 8 mg/ml and frozen on graphene
694 oxide grids (GO on Quantifoils R1.2/1.3, Cu, 400 mesh, Electron Microscopy Sciences) with 30
695 sec wait time, blot force of 0, and blot time of 2.5-3 s. Fluorinated Fos-Choline-8 (Anatrace #
696 F300F) was added to sample immediately prior to freezing to a final concentration of 3 mM. GO
697 grids, high sample concentration and fluorinated Fos-Choline-8 were necessary to prevent freeze-
698 denaturation, ensure high particle count per micrograph and prevent orientation bias. 11,871
699 micrographs were collected at pixel size 0.718 Å using a Thermo Fisher Scientific Glacios 2
700 microscope operating at 200 kV and equipped with a Thermo Fisher Scientific Falcon 4i camera

701 using a total dose of 44.89 e-/Å2. Automated data collection was performed using the EPU
702 software (Thermo Fisher Scientific) and images were written in the EER frame format.
703 Micrographs were preprocessed using cryoSPARC Live[66], including motion and CTF correction.
704 Briefly, particles were picked with Topaz[67] after training the neural network with a subset of
705 particles first picked with blob picker. Picked particles were subjected to 3 rounds of 2D
706 classification to obtain a final particle stack of 317,792 particles. These were then extracted from
707 micrographs using a box size of 540 pix. Maps containing one or two copies of 10E8 Fab were
708 separated using heterogenous reconstruction and 3D classification tasks. A class with 7,964
709 particles containing two copies of 10E8 was refined to 4.3Å resolution. A class with 111,002
710 particles containing single 10E8 was examined with 3D variability analysis[68]. Further
711 classification resulted in final, cleaned particle stack containing 63,366 particles which was then
712 subjected to Non-Uniform Refinement[69] and used for atomic model building. Data collection and
713 processing stats are summarized in Supplementary Table 1. Atomic model building was initiated
714 by docking in available structures of 10E8 Fab (PDB 4G6F), BG18 Fab (PDB 6DFG), VRC01
715 Fab (PDB 3NGB) and an AlphaFold3[70] -generated model of the trimer into the map using
716 ChimeraX[71]. Manual adjustment was done using Coot[72] and further refinement was done using
717 Phenix Real Space Refine[73] and Rosetta Relax[74]. Final model statistics are summarized in
718 Supplementary Table 1.

719 The soluble gp140 (MD39.3) cryo-EM structure was done as follows: VRC01, BG18 and
720 3BC315 Fabs were added at 4.3X molar excess to purified Env glycoprotein. The complex was
721 purified using a HiLoad Superdex 200 16/600 pg column (Cytiva) and concentrated to 10 mg/ml.
722 Samples were vitrified using a Thermo Fisher Scientific Vitrobot Mark IV operating at 100%
723 humidity, 4°C and 3-6 s blot times, on UltrAuFoil 1.2/1.3-300 holey gold film grids (Electron
724 Microscopy Sciences). Prior to grid application, lauryl maltose neopentyl glycol (LMNG) was
725 added to a final concentration of 0.005 mM. Imaging was performed using the same microscope
726 and conditions as for Env gp151 MPER ND complex. After initial cryoSPARC particle picking
727 using Blob Picker, templates were selected from 2D classification and used for Template Picker.
728 A total of 886,907 particles were extracted using a box size of 576 downsampled to 144. After

729 additional rounds of 2D classification, an Ab Initio Reconstruction was performed, followed by
730 Non-Uniform refinement. A single 3BC315 Fab was visible in the C1 reconstruction. A mask was
731 created over 3BC315 and focused 3D classification performed to remove trimers with no 3BC315
732 particles. A final stack of 243,503 were re-extracted and downsampled to box size 400 (resulting
733 in pixel size of 1.034 Å) and subjected to Non-Uniform Refinement which resulted in a 3.1 Å
734 reconstruction. Model building was performed as above and final model statistics are summarized
735 in Supplementary Table 1.
736 Maps and models have been deposited to the EMDB and PDB, respectively, under the
737 accession codes listed in Supplementary Table 1.
738

739 **Acknowledgements**
740 We thank Nicole Doria-Rose for providing the VRC01 expressing Ramos cell line. We thank Brian
741 Briney for providing access to Illumina NextSeq 2000 sequencer. We thank Daniel Murin for
742 providing Ebola GP specific antibodies.
743

744 **Funding**
745 This work was supported by National Institute of Allergy and Infectious Diseases UM1 AI144462
746 (Scripps Consortium for HIV/AIDS Vaccine Development; to J.C.P., T.S., A.B.W., and W.R.S),
747 R01 AI147826 (to W.R.S.); Bill and Melinda Gates Foundation Collaboration for AIDS Vaccine
748 Discovery awards (INV-007522 and INV-008813 for the IAVI NAC Center to A.B.W. and
749 W.R.S.; and INV-002916 to A.B.W.); the IAVI Neutralizing Antibody Center (to A.B.W. and
750 W.R.S.); and the Alexander von Humboldt Foundation (T.S.).
751

752 **Competing interests**: J.M.S and W.R.S. are inventors on a patent for the BG505 MD39 and N332-
753 GT5 immunogens (US11203617B2 and US20230190914A1). S.H. and W.R.S. are employees and
754 shareholders of Moderna, Inc. All other authors declare no competing interests.
755

Author contributions: K.R. designed nanodisc assembly workflow, performed cryo-EM imaging, data processing and structural analysis, and wrote the manuscript. A.L. and O.K. established conditions and conducted SPR assays. G.O. Supervised cryo-EM imaging and data processing and built 3D models. C.F. performed and J.H.L. and D.S. supervised establishing conditions for mouse B cell FACS experiments. J.M.S., O.S. and T.S. contributed to immunogen design. S.B. and J.K.D. performed, and J.R.Y. and J.C.P. supervised mass spectrometry glycan profiling. P.J.M. and M.S. performed, and S.C. supervised NHP B cell FACS analysis. S.W. and A.G. contributed, and G.O. and A.B.W. supervised cryo-EM imaging, data processing and model building. D.L. performed nanodisc assembly reactions. P.K. and S.T. performed mouse immunizations. D.L., E.G., R.T., S.E., N.A., D.G. and M.K. produced purified proteins. W-H.L. contributed to cryo-EM sample preparation. S.H. provided mRNA immunogens. T.S., A.B.W. and W.R.S. supervised the study. G.O., T.S., A.B.W. and W.R.S. edited the manuscript. All authors reviewed the manuscript.

771 **Figure legends**

772

773 **Figure 1.** Nanodisc use in different steps in iterative rational vaccine design. Analytical methods
774 that can directly use nanodiscs as sample material are highlighted.

775

776 **Figure 2.** HIV Env constructs used for method development and general overview of the nanodisc
777 assembly workflow. a) Naming and gene organization of the glycoprotein constructs used for
778 nanodisc assembly. Introduced mutations and intracellular elements are indicated. ND refers to
779 constructs made for nanodisc platform. b) Schematic overview of HIV Env constructs and MPER
780 targeting antibody 10E8 binding. c) Key steps of the 5-day workflow for glycoprotein nanodisc
781 assembly. Glycoprotein was extracted with detergent from cell surface and bound to affinity
782 matrix. Disc assembly was performed "in-batch" while bound to affinity purification matrix.
783 Assembled discs were then eluted for final SEC polishing purification, followed by quality control
784 steps before subjecting to final analytical methods (SPR, FACS, cryo-EM).

785

786 **Figure 3.** Different SPR modalities and kinetic analyses of GP nanodiscs. a) Schematic
787 illustrations of three SPR modalities used throughout the study and their strengths and weaknesses.
788 b) Affinity of MPER targeting 10E8 antibody to Env gp151 ND as measured with modalities A
789 and B. Affinities with modality A were measured after storing the sample either 1 week (white), 1
790 month (grey) or 3 months (black) at 4°C. c) Affinity of 10E8 against Env constructs using modality
791 A. d) SPR data presented in (c), showing increase in affinity originating from reduced off-rate in
792 Env gp151 MPER ND. e) Modality C was used to scout Ebola specific EBOV-296 and EBOV-
793 13C6 IgG epitope accessibility in EBOV GP nanodiscs. Data shows binding of two anti -Ebola
794 antibodies targeting the glycan cap (EBOV-296 and 13C6). Env gp151 ND and anti-HIV MPER
795 antibody PGZL1 were used as a negative controls.

796

797 **Figure 4.** HIV Env nanodisc FACS probe validation and pilot use in pre-clinical mouse model. a)
798 Nanodiscs were tested for binding to HIV MPER bnAbs 10E8 and DH511 and gp120-specific

799 bnAb BG18 coupled to FACS compensation beads, B6 mouse splenocytes were used as negative
800 control cells, and VRC01 expressing Ramos cells as positive control cells. Empty nanodiscs were
801 assembled with either DOPC lipids (blue) or a mixture of neutral and charged lipids (green). b)
802 Memory ($CD19^{+}IgM^{-}IgD^{-}$) and naïve ($CD19^{+}IgM^{+}IgD^{+}$) B cells from mice 6 weeks after
803 immunization with mRNA-LNPs encoding Env gp151 MPER ND nanodisc were analyzed by flow
804 cytometry. Antigen-specific (Env gp151 MPER ND^{++}) and epitope-specific (KO^{-}) B cells were
805 detected using immunogen-matched WT and 10E8-epitope KO nanodisc probes and WT
806 $nanodisc^{++}$ cells were sorted for BCR sequencing. The complete gating strategy is shown in
807 supplementary Fig. 3. c) Percent antigen-specific memory B cells in the naïve vs. memory
808 compartments of each immunized mouse (top), and proportion of 10E8 epitope-specific (KO^{-})
809 cells within each antigen-specific population. Paired t-test, *$p < 0.05$, ns: $p > 0.05$. d) Sorted cells
810 were sequenced and selected antibodies were purified for affinity measurement by SPR using
811 modality B.
812
813 **Figure 5.** HIV Env nanodisc probe validation for sorting NHP cells. a) Flow cytometry plots
814 showing $CD20^{+}IgD^{-}$ memory B cells stained with Env gp151 ND nanodisc on two different
815 fluorophores. Pre-immunization and 2-weeks post-immunization PBMCs from the same RM are
816 shown and the frequency of $Nanodisc^{++}$ cells of IgD^{-} cells is listed. b) Flow cytometry plots
817 showing $CD20^{+}IgG^{+}$ memory B cells stained with either soluble Env gp140 protein or Env gp151
818 ND nanodisc on two different fluorophores. PBMCs from two different RMs 4-weeks post mRNA
819 Env gp151 immunization were split and stained with Env gp140 protein tetramers (left column)
820 or matching nanodisc Env gp151 ND tetramers (right column). The frequency of $tetramer^{++}$ cells
821 of IgG^{+} cells is listed for each plot.
822
823 **Figure 6.** Structure of Env gp151 MPER ND in complex with bnAbs BG18, VRC01 and 10E8
824 resolved by cryo-EM. a) Low pass filtered maps of different Fab occupancy states and the location
825 of the bilayer. BG18 Fab is highlighted in green, VRC01 in pink and 10E8 in blue. b) 90° clockwise
826 rotated side views showing the Env tilt angle in relation to lipid bilayer surface. c) Top view and

827 side views of highest resolution maps of both 10E8 occupancy states. Densities are highlighted as
828 follows: gp120 in blue, gp41 in orange, BG18 in green, VRC01 in pink, HC of 10E8 in white, LC
829 of 10E8 in dark grey and MPER peptide in red. d) Highest resolution reconstruction with single
830 10E8 was used for model building. Insets show interfaces of the three bound bnAbs and key amino
831 acid and glycan interactions with BG18 HC (dark green) and LC (light green) in insets 1-2, VRC01
832 HC (magenta) and LC (pink) in insets 3-4, and 10E8 HC (white) and LC (dark grey) in insets 5-7.
833 Glycans are highlighted in purple. Insets 2 and 4 exemplify the electron density used to built
834 interacting glycans (transparent blue. e) Epitope-paratope analysis of 10E8 binding interface
835 shown in d. Contacting residues are separated into three components corresponding insets 5-7. f)
836 Binding pocket of 3BC315 (salmon) CDRH3 with key interactions highlighted. g) gp41 protomer
837 distance analysis in the nanodisc complex structure with 10E8 Fab, and soluble Env structure with
838 3BC315 showing widened interface between protomers A and B due to antibody binding.
839

840 **Figures**

841

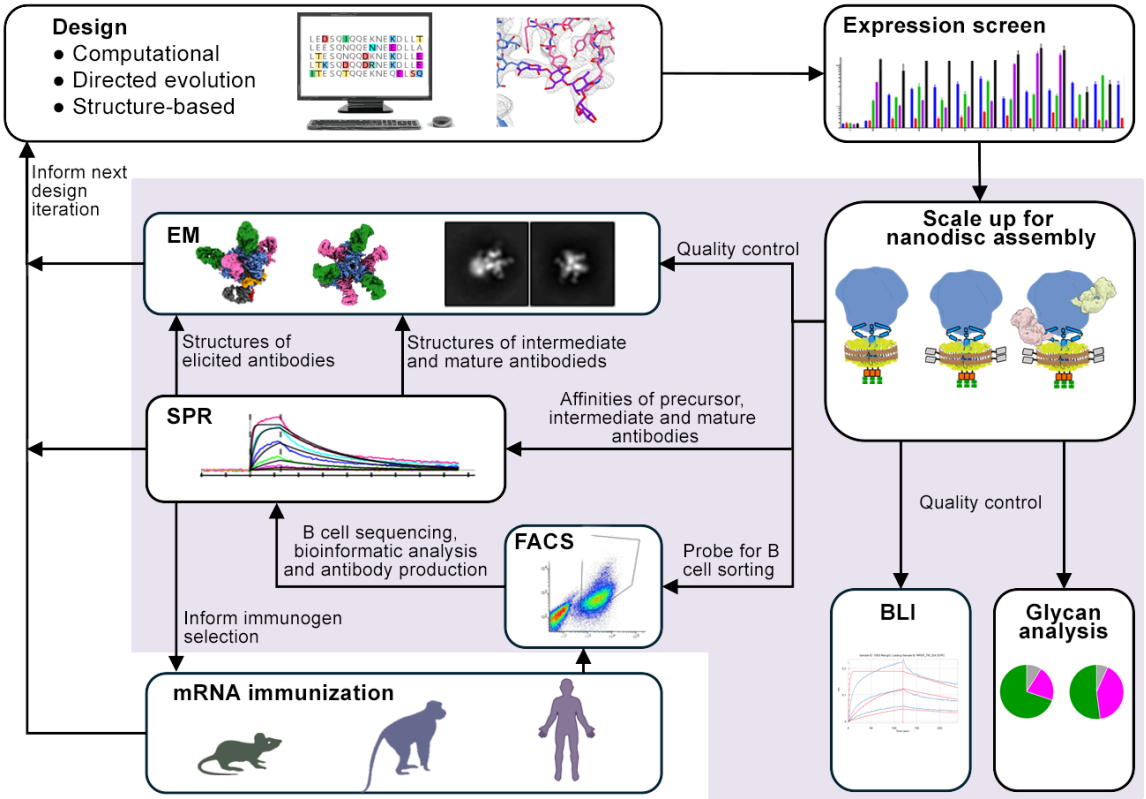

842

843 **Figure 1**

844

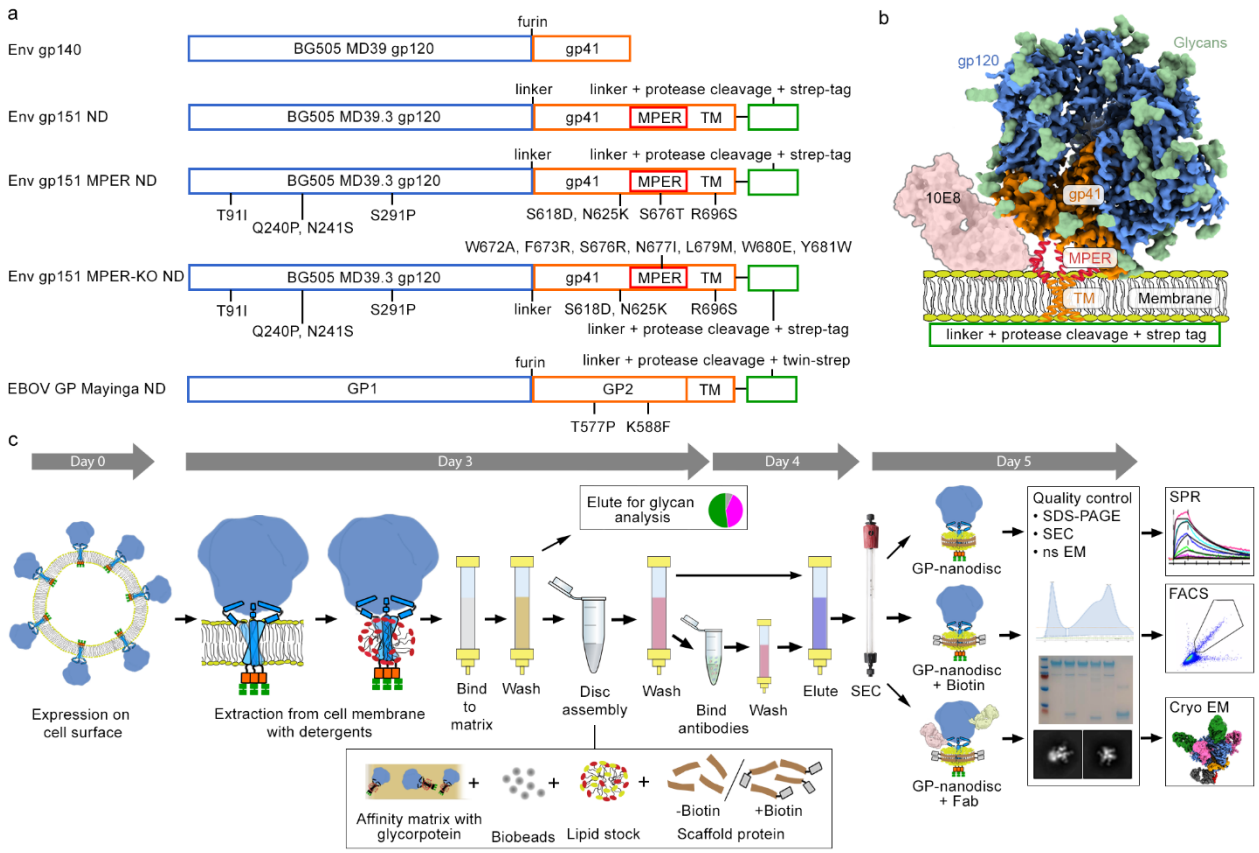

845

846 **Figure 2**

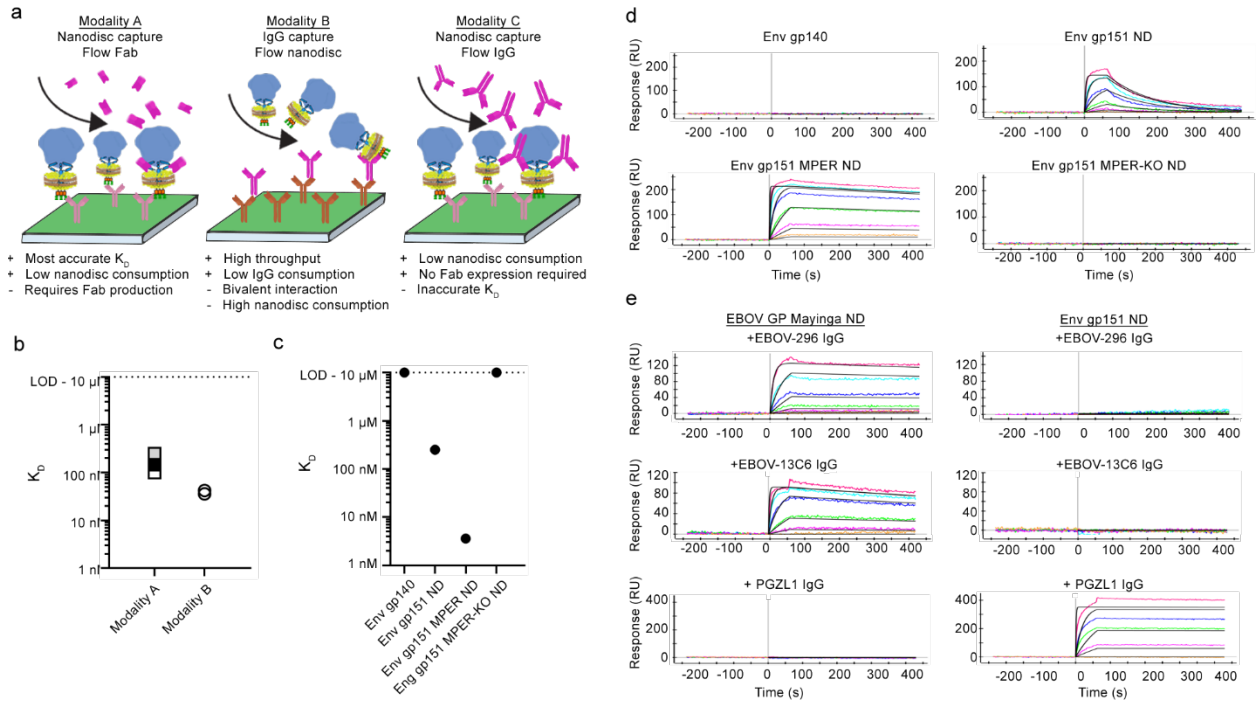
a
Modality A
Nanodisc capture
Flow Fab
+ Most accurate K_D
+ Low nanodisc consumption
- Requires Fab production
Modality B
IgG capture
Flow nanodisc
+ High throughput
+ Low IgG consumption
- Bivalent interaction
- High nanodisc consumption
Modality C
Nanodisc capture
Flow IgG
+ Low nanodisc consumption
+ No Fab expression required
- Inaccurate K_D
b
LOD - 10 µM
1 µM
100 nM
10 nM
1 nM
K_D
Modality A
Modality B
c
LOD - 10 µM
1 µM
100 nM
10 nM
1 nM
K_D
Env gp140
Env gp151 ND
Env gp151 MPER ND
Eng gp151 MPER-KO ND
d
Env gp140
Env gp151 ND
Env gp151 MPER ND
Env gp151 MPER-KO ND
Response (RU)
Time (s)
e
EBOV GP Mayinga ND
Env gp151 ND
+EBOV-296 IgG
+EBOV-13C6 IgG
+ PGZL1 IgG
Response (RU)
Time (s)

Figure 3

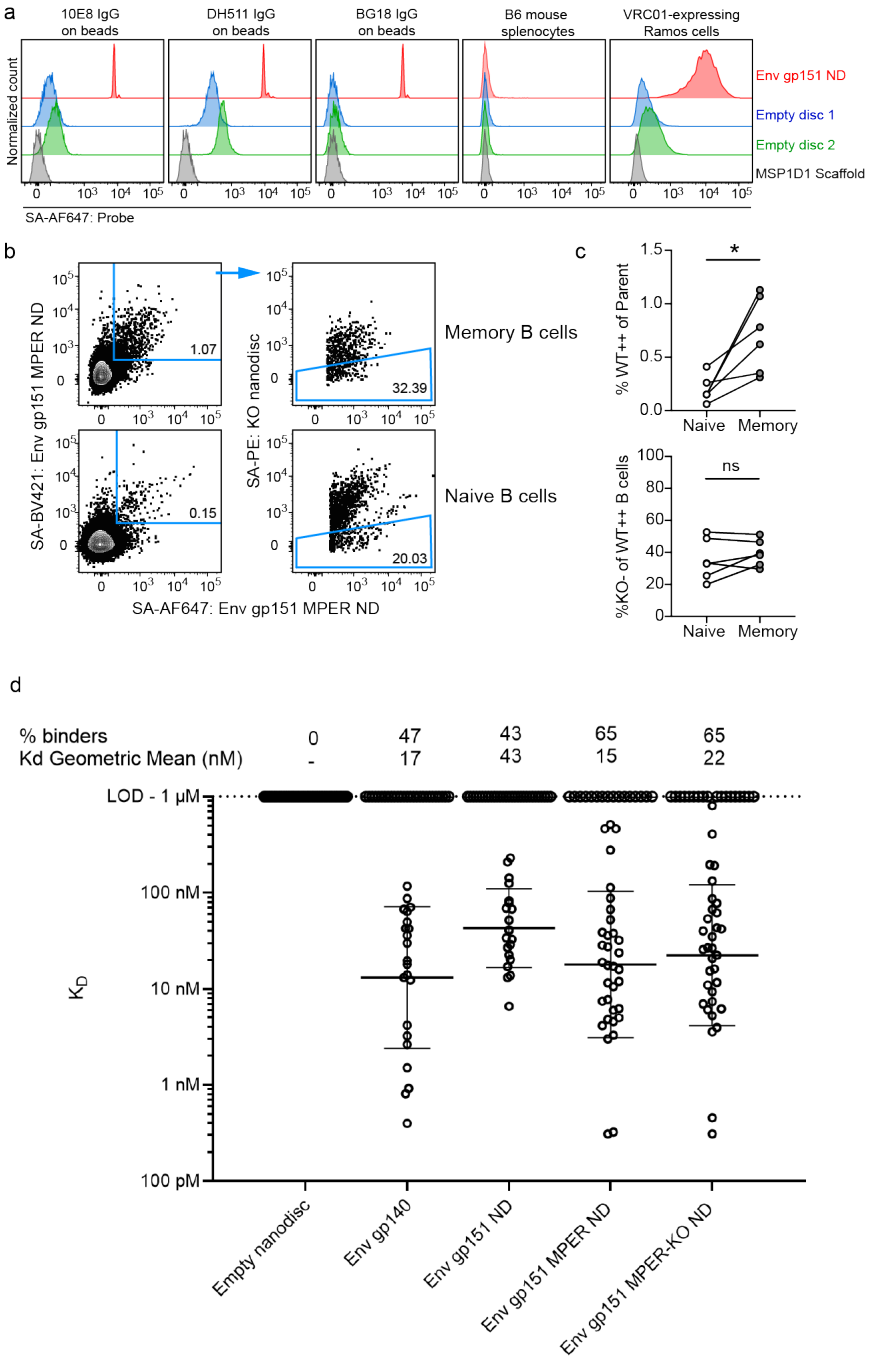
a
10E8 IgG on beads
DH511 IgG on beads
BG18 IgG on beads
B6 mouse splenocytes
VRC01-expressing Ramos cells
Normalized count
Env gp151 ND
Empty disc 1
Empty disc 2
MSP1D1 Scaffold
SA-AF647: Probe
b
SA-BV421: Env gp151 MPER ND
SA-PE: KO nanodisc
SA-AF647: Env gp151 MPER ND
1.07
0.15
32.39
20.03
Memory B cells
Naive B cells
c
% WT++ of Parent
%KO- of WT++ B cells
Naive
Memory
*
ns
d
% binders
Kd Geometric Mean (nM)
0
47
43
65
65
-
17
43
15
22
LOD - 1 μM
100 nM
10 nM
1 nM
100 pM
K_D
Empty nanodisc
Env gp140
Env gp151 ND
Env gp151 MPER ND
Env gp151 MPER-KO ND

Figure 4

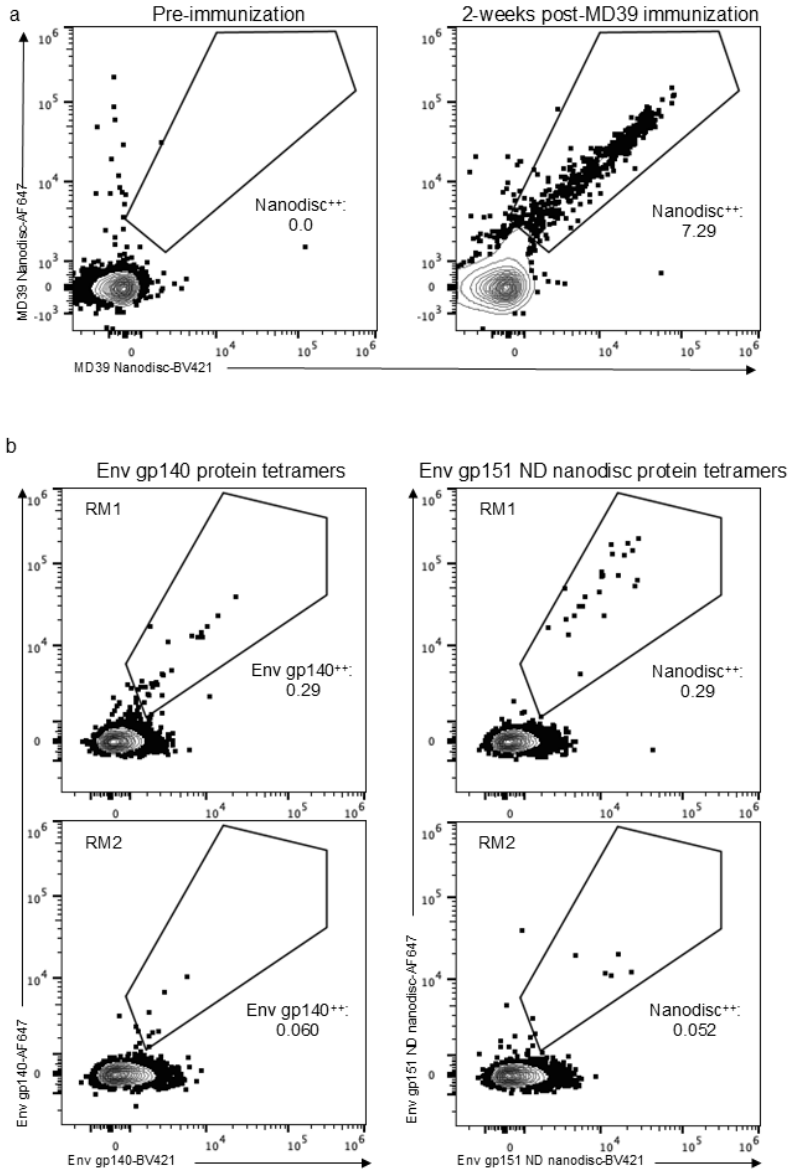
a
Pre-immunization
2-weeks post-MD39 immunization
Nanodisc++:
0.0
Nanodisc++:
7.29
MD39 Nanodisc-AF647
MD39 Nanodisc-BV421
b
Env gp140 protein tetramers
Env gp151 ND nanodisc protein tetramers
RM1
Env gp140++:
0.29
Nanodisc++:
0.29
RM2
Env gp140++:
0.060
Nanodisc++:
0.052
Env gp140-AF647
Env gp140-BV421
Env gp151 ND nanodisc-AF647
Env gp151 ND nanodisc-BV421

Figure 5

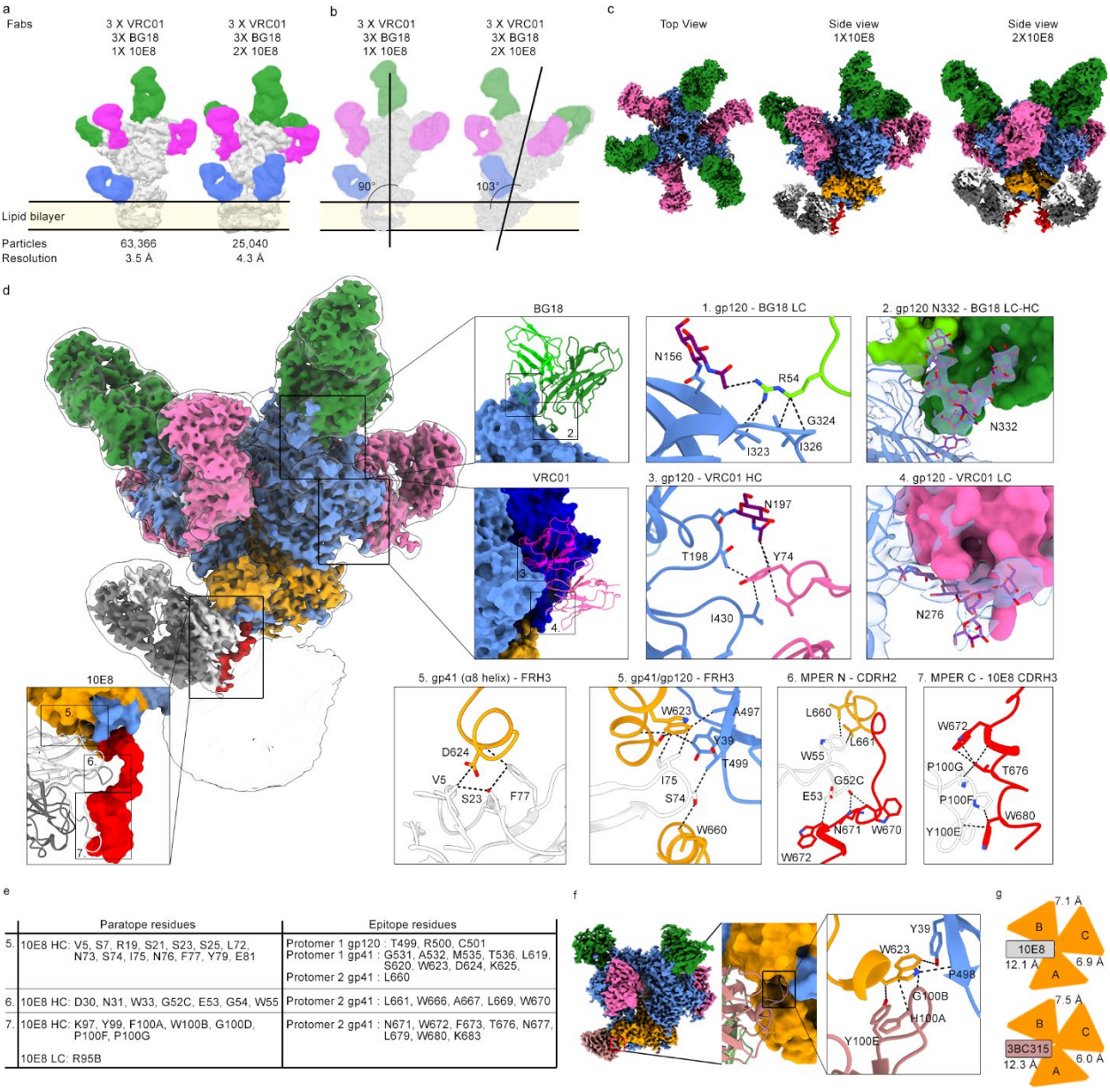

	Paratope residues	Epitope residues
5.	10E8 HC: V5, S7, R19, S21, S23, S25, L72, N73, S74, I75, N76, F77, Y79, E81	Protomer 1 gp120 : T499, R500, C501 Protomer 1 gp41 : G531, A532, M535, T536, L619, S620, W623, D624, K625, Protomer 2 gp41 : L660
6.	10E8 HC: D30, N31, W33, G52C, E53, G54, W55	Protomer 2 gp41 : L661, W666, A667, L669, W670
7.	10E8 HC: K97, Y99, F100A, W100B, G100D, P100F, P100G 10E8 LC: R95B	Protomer 2 gp41 : N671, W672, F673, T676, N677, L679, W680, K683

Figure 6

856 **References**

857 1. Bayburt, T.H., Grinkova, Y.V. & Sligar, S.G. Self-assembly of discoidal phospholipid
858 bilayer nanoparticles with membrane scaffold proteins. *Nano Letters* **2**, 853-856 (2002).
859 2. Dorr, J.M. et al. The styrene-maleic acid copolymer: a versatile tool in membrane
860 research. *Eur Biophys J* **45**, 3-21 (2016).
861 3. Carlson, M.L. et al. The Peptidisc, a simple method for stabilizing membrane proteins in
862 detergent-free solution. *Elife* **7** (2018).
863 4. Frauenfeld, J. et al. A saposin-lipoprotein nanoparticle system for membrane proteins.
864 *Nat Methods* **13**, 345-351 (2016).
865 5. Pettersen, J.M., Yang, Y. & Robinson, A.S. Advances in nanodisc platforms for
866 membrane protein purification. *Trends Biotechnol* **41**, 1041-1054 (2023).
867 6. Sligar, S.G. & Denisov, I.G. Nanodiscs: A toolkit for membrane protein science. *Protein*
868 *Sci* **30**, 297-315 (2021).
869 7. Denisov, I.G. & Sligar, S.G. Nanodiscs for structural and functional studies of membrane
870 proteins. *Nat Struct Mol Biol* **23**, 481-486 (2016).
871 8. Trahey, M. et al. Applications of Lipid Nanodiscs for the Study of Membrane Proteins by
872 Surface Plasmon Resonance. *Curr Protoc Protein Sci* **81**, 29 13 21-29 13 16 (2015).
873 9. Bocquet, N. et al. Real-time monitoring of binding events on a thermostabilized human
874 A2A receptor embedded in a lipid bilayer by surface plasmon resonance. *Biochim*
875 *Biophys Acta* **1848**, 1224-1233 (2015).
876 10. Gluck, J.M., Koenig, B.W. & Willbold, D. Nanodiscs allow the use of integral membrane
877 proteins as analytes in surface plasmon resonance studies. *Anal Biochem* **408**, 46-52
878 (2011).
879 11. Wang, M.Y. et al. SARS-CoV-2: Structure, Biology, and Structure-Based Therapeutics
880 Development. *Front Cell Infect Microbiol* **10**, 587269 (2020).
881 12. Pallesen, J. et al. Immunogenicity and structures of a rationally designed prefusion
882 MERS-CoV spike antigen. *Proc Natl Acad Sci U S A* **114**, E7348-E7357 (2017).
883 13. Kirchdoerfer, R.N. et al. Pre-fusion structure of a human coronavirus spike protein.
884 *Nature* **531**, 118-121 (2016).
885 14. Shepherd, B.O., Chang, D., Vasan, S., Ake, J. & Modjarrad, K. HIV and SARS-CoV-2:
886 Tracing a Path of Vaccine Research and Development. *Curr HIV/AIDS Rep* **19**, 86-93
887 (2022).
888 15. Pardi, N., Hogan, M.J., Porter, F.W. & Weissman, D. mRNA vaccines - a new era in
889 vaccinology. *Nat Rev Drug Discov* **17**, 261-279 (2018).
890 16. Chaudhary, N., Weissman, D. & Whitehead, K.A. mRNA vaccines for infectious
891 diseases: principles, delivery and clinical translation. *Nat Rev Drug Discov* **20**, 817-838
892 (2021).
893 17. Guenaga, J. et al. mRNA lipid nanoparticles expressing cell-surface cleavage
894 independent HIV Env trimers elicit autologous tier-2 neutralizing antibodies. *Front*
895 *Immunol* **15**, 1426232 (2024).

896 18. Benton, D.J. et al. Influenza hemagglutinin membrane anchor. *Proc Natl Acad Sci U S A*
897 **115**, 10112-10117 (2018).
898 19. Lopez, C.A., Alam, S.M., Derdeyn, C.A., Haynes, B.F. & Gnanakaran, S. Influence of
899 membrane on the antigen presentation of the HIV-1 envelope membrane proximal
900 external region (MPER). *Curr Opin Struct Biol* **88**, 102897 (2024).
901 20. Liu, H., Su, X., Si, L., Lu, L. & Jiang, S. The development of HIV vaccines targeting
902 gp41 membrane-proximal external region (MPER): challenges and prospects. *Protein*
903 *Cell* **9**, 596-615 (2018).
904 21. Guthmiller, J.J. et al. Broadly neutralizing antibodies target a haemagglutinin anchor
905 epitope. *Nature* **602**, 314-320 (2022).
906 22. Zhang, L. et al. An MPER antibody neutralizes HIV-1 using germline features shared
907 among donors. *Nat Commun* **10**, 5389 (2019).
908 23. Krebs, S.J. et al. Longitudinal Analysis Reveals Early Development of Three MPER-
909 Directed Neutralizing Antibody Lineages from an HIV-1-Infected Individual. *Immunity*
910 **50**, 677-691 e613 (2019).
911 24. Schiffner, T. et al. Vaccination induces broadly neutralizing antibody precursors to HIV
912 gp41. *Nat Immunol* **25**, 1073-1082 (2024).
913 25. Williams, W.B. et al. Vaccine induction of heterologous HIV-1-neutralizing antibody B
914 cell lineages in humans. *Cell* **187**, 2919-2934 e2920 (2024).
915 26. Cao, L. et al. Differential processing of HIV envelope glycans on the virus and soluble
916 recombinant trimer. *Nat Commun* **9**, 3693 (2018).
917 27. Rantalainen, K. et al. Co-evolution of HIV Envelope and Apex-Targeting Neutralizing
918 Antibody Lineage Provides Benchmarks for Vaccine Design. *Cell Rep* **23**, 3249-3261
919 (2018).
920 28. Torrents de la Pena, A. et al. Similarities and differences between native HIV-1 envelope
921 glycoprotein trimers and stabilized soluble trimer mimetics. *PLoS Pathog* **15**, e1007920
922 (2019).
923 29. Rantalainen, K. et al. HIV-1 Envelope and MPER Antibody Structures in Lipid
924 Assemblies. *Cell Rep* **31**, 107583 (2020).
925 30. Nakatani-Webster, E., Hu, S.L., Atkins, W.M. & Catalano, C.E. Assembly and
926 characterization of gp160-nanodiscs: A new platform for biochemical characterization of
927 HIV envelope spikes. *J Virol Methods* **226**, 15-24 (2015).
928 31. Bhattacharya, P. et al. Nanodisc-incorporated hemagglutinin provides protective
929 immunity against influenza virus infection. *J Virol* **84**, 361-371 (2010).
930 32. Mabrouk, M.T. et al. Circularized Nanodiscs for Multivalent Mosaic Display of SARS-
931 CoV-2 Spike Protein Antigens. *Vaccines (Basel)* **11** (2023).
932 33. Yang, S. et al. Dynamic HIV-1 spike motion creates vulnerability for its membrane-
933 bound tripod to antibody attack. *Nat Commun* **13**, 6393 (2022).
934 34. Steichen, J.M. et al. HIV Vaccine Design to Target Germline Precursors of Glycan-
935 Dependent Broadly Neutralizing Antibodies. *Immunity* **45**, 483-496 (2016).

936 35. Willis, J.R. et al. Human immunoglobulin repertoire analysis guides design of vaccine
937 priming immunogens targeting HIV V2-apex broadly neutralizing antibody precursors.
938 *Immunity* **55**, 2149-2167 e2149 (2022).
939 36. Puthenveetil, R., Nguyen, K. & Vinogradova, O. Nanodiscs and Solution NMR:
940 preparation, application and challenges. *Nanotechnol Rev* **6**, 111-126 (2017).
941 37. Gu, S., Huang, M. & Handel, T.M. On-bead purification and nanodisc reconstitution of
942 human chemokine receptor complexes for structural and biophysical studies. *STAR*
943 *Protoc* **4**, 102460 (2023).
944 38. Dev, J. et al. Structural basis for membrane anchoring of HIV-1 envelope spike. *Science*
945 **353**, 172-175 (2016).
946 39. Rutten, L. et al. Structure-Based Design of Prefusion-Stabilized Filovirus Glycoprotein
947 Trimers. *Cell Rep* **30**, 4540-4550 e4543 (2020).
948 40. Steichen, J.M. et al. A generalized HIV vaccine design strategy for priming of broadly
949 neutralizing antibody responses. *Science* **366** (2019).
950 41. Xie, Z. et al. mRNA-LNP HIV-1 trimer boosters elicit precursors to broad neutralizing
951 antibodies. *Science* **384**, eadk0582 (2024).
952 42. Baboo, S. et al. DeGlyPHER: An Ultrasensitive Method for the Analysis of Viral Spike
953 N-Glycoforms. *Anal Chem* **93**, 13651-13657 (2021).
954 43. Hossain, M.A. et al. B cells expressing IgM B cell receptors of HIV-1 neutralizing
955 antibodies discriminate antigen affinities by sensing binding association rates. *Cell Rep*
956 **39**, 111021 (2022).
957 44. Steichen, J.M. et al. Vaccine priming of rare HIV broadly neutralizing antibody
958 precursors in nonhuman primates. *Science* **384**, eadj8321 (2024).
959 45. Vazquez Bernat, N. et al. Rhesus and cynomolgus macaque immunoglobulin heavy-chain
960 genotyping yields comprehensive databases of germline VDJ alleles. *Immunity* **54**, 355-
961 366 e354 (2021).
962 46. Chernyshev, M., Kaduk, M., Corcoran, M. & Karlsson Hedestam, G.B. VDJ Gene Usage
963 in IgM Repertoires of Rhesus and Cynomolgus Macaques. *Front Immunol* **12**, 815680
964 (2021).
965 47. Phung, I. et al. A combined adjuvant approach primes robust germinal center responses
966 and humoral immunity in non-human primates. *Nat Commun* **14**, 7107 (2023).
967 48. Ramezani-Rad, P. et al. Vaccination with mRNA-encoded membrane-bound HIV
968 Envelope trimer induces neutralizing antibodies in animal models. *bioRxiv* (2025).
969 49. Irimia, A. et al. Lipid interactions and angle of approach to the HIV-1 viral membrane of
970 broadly neutralizing antibody 10E8: Insights for vaccine and therapeutic design. *PLoS*
971 *Pathog* **13**, e1006212 (2017).
972 50. Soto, C. et al. Developmental Pathway of the MPER-Directed HIV-1-Neutralizing
973 Antibody 10E8. *PLoS One* **11**, e0157409 (2016).
974 51. Rujas, E. et al. Structural basis for broad neutralization of HIV-1 through the molecular
975 recognition of 10E8 helical epitope at the membrane interface. *Sci Rep* **6**, 38177 (2016).
976 52. Huang, J. et al. Broad and potent neutralization of HIV-1 by a gp41-specific human
977 antibody. *Nature* **491**, 406-412 (2012).

53. Lee, J.H. et al. Antibodies to a conformational epitope on gp41 neutralize HIV-1 by destabilizing the Env spike. *Nat Commun* **6**, 8167 (2015).
54. Pancera, M. et al. Structure and immune recognition of trimeric pre-fusion HIV-1 Env. *Nature* **514**, 455-461 (2014).
55. Ray, R. et al. Affinity gaps among B cells in germinal centers drive the selection of MPER precursors. *Nature Immunology* **25** (2024).
56. Cottrell, C.A. et al. Heterologous prime-boost vaccination drives early maturation of HIV broadly neutralizing antibody precursors in humanized mice. *Sci Transl Med* **16**, eadn0223 (2024).
57. Antanasijevic, A. et al. Polyclonal antibody responses to HIV Env immunogens resolved using cryoEM. *Nat Commun* **12**, 4817 (2021).
58. Barnes, C.O. et al. Structural characterization of a highly-potent V3-glycan broadly neutralizing antibody bound to natively-glycosylated HIV-1 envelope. *Nat Commun* **9**, 1251 (2018).
59. He, L., Diedrich, J., Chu, Y.Y. & Yates, J.R., 3rd Extracting Accurate Precursor Information for Tandem Mass Spectra by RawConverter. *Anal Chem* **87**, 11361-11367 (2015).
60. Xu, T. et al. ProLuCID: An improved SEQUEST-like algorithm with enhanced sensitivity and specificity. *J Proteomics* **129**, 16-24 (2015).
61. Tabb, D.L., McDonald, W.H. & Yates, J.R., 3rd DTASelect and Contrast: tools for assembling and comparing protein identifications from shotgun proteomics. *J Proteome Res* **1**, 21-26 (2002).
62. Peng, J., Elias, J.E., Thoreen, C.C., Licklider, L.J. & Gygi, S.P. Evaluation of multidimensional chromatography coupled with tandem mass spectrometry (LC/LC-MS/MS) for large-scale protein analysis: the yeast proteome. *J Proteome Res* **2**, 43-50 (2003).
63. Park, S.K., Venable, J.D., Xu, T. & Yates, J.R., 3rd A quantitative analysis software tool for mass spectrometry-based proteomics. *Nat Methods* **5**, 319-322 (2008).
64. Hurtado, J. et al. Efficient isolation of rare B cells using next-generation antigen barcoding. *Front Cell Infect Microbiol* **12**, 962945 (2022).
65. Breden, F. et al. Reproducibility and Reuse of Adaptive Immune Receptor Repertoire Data. *Front Immunol* **8**, 1418 (2017).
66. Punjani, A., Rubinstein, J.L., Fleet, D.J. & Brubaker, M.A. cryoSPARC: algorithms for rapid unsupervised cryo-EM structure determination. *Nat Methods* **14**, 290-296 (2017).
67. Bepler, T. et al. Positive-unlabeled convolutional neural networks for particle picking in cryo-electron micrographs. *Nat Methods* **16**, 1153-1160 (2019).
68. Punjani, A. & Fleet, D.J. 3D variability analysis: Resolving continuous flexibility and discrete heterogeneity from single particle cryo-EM. *J Struct Biol* **213**, 107702 (2021).
69. Punjani, A., Zhang, H. & Fleet, D.J. Non-uniform refinement: adaptive regularization improves single-particle cryo-EM reconstruction. *Nat Methods* **17**, 1214-1221 (2020).
70. Abramson, J. et al. Accurate structure prediction of biomolecular interactions with AlphaFold 3. *Nature* **630**, 493-500 (2024).

1020 71. Pettersen, E.F. et al. UCSF ChimeraX: Structure visualization for researchers, educators,
1021 and developers. *Protein Sci* **30**, 70-82 (2021).
1022 72. Casanal, A., Lohkamp, B. & Emsley, P. Current developments in Coot for
1023 macromolecular model building of Electron Cryo-microscopy and Crystallographic Data.
1024 *Protein Sci* **29**, 1069-1078 (2020).
1025 73. Afonine, P.V. et al. Real-space refinement in PHENIX for cryo-EM and crystallography.
1026 *Acta Crystallogr D Struct Biol* **74**, 531-544 (2018).
1027 74. Conway, P., Tyka, M.D., DiMaio, F., Konerding, D.E. & Baker, D. Relaxation of
1028 backbone bond geometry improves protein energy landscape modeling. *Protein Sci* **23**,
1029 47-55 (2014).
1030

1031